

3-8-2022

Differential recognition of canonical NF- κ B dimers by Importin α 3

Tyler J. Florio

Ravi K Lokareddy


Daniel P Yeggoni

Rajeshwer S Sankhala

Connor A Ott

See next page for additional authors

Follow this and additional works at: <https://jdc.jefferson.edu/bmpfp>

 Part of the [Medical Biochemistry Commons](#), and the [Medical Molecular Biology Commons](#)



[Let us know how access to this document benefits you](#)

This Article is brought to you for free and open access by the Jefferson Digital Commons. The Jefferson Digital Commons is a service of Thomas Jefferson University's [Center for Teaching and Learning \(CTL\)](#). The Commons is a showcase for Jefferson books and journals, peer-reviewed scholarly publications, unique historical collections from the University archives, and teaching tools. The Jefferson Digital Commons allows researchers and interested readers anywhere in the world to learn about and keep up to date with Jefferson scholarship. This article has been accepted for inclusion in Department of Biochemistry and Molecular Biology Faculty Papers by an authorized administrator of the Jefferson Digital Commons. For more information, please contact: JeffersonDigitalCommons@jefferson.edu.

Authors

Tyler J. Florio, Ravi K Lokareddy, Daniel P Yeggoni, Rajeshwer S Sankhala, Connor A Ott, Richard E Gillilan, and Gino Cingolani

Differential recognition of canonical NF- κ B dimers by Importin α 3

Tyler J. Florio¹, Ravi K. Lokareddy¹, Daniel P. Yeggoni¹, Rajeshwer S. Sankhala², Connor A. Ott ¹, Richard E. Gillilan ³ & Gino Cingolani ¹✉

Nuclear translocation of the p50/p65 heterodimer is essential for NF- κ B signaling. In unstimulated cells, p50/p65 is retained by the inhibitor I κ B α in the cytoplasm that masks the p65-nuclear localization sequence (NLS). Upon activation, p50/p65 is translocated into the nucleus by the adapter importin α 3 and the receptor importin β . Here, we describe a bipartite NLS in p50/p65, analogous to nucleoplasmin NLS but exposed in trans. Importin α 3 accommodates the p50- and p65-NLSs at the major and minor NLS-binding pockets, respectively. The p50-NLS is the predominant binding determinant, while the p65-NLS induces a conformational change in the Armadillo 7 of importin α 3 that stabilizes a helical conformation of the p65-NLS. Neither conformational change was observed for importin α 1, which makes fewer bonds with the p50/p65 NLSs, explaining the preference for α 3. We propose that importin α 3 discriminates between the transcriptionally active p50/p65 heterodimer and p50/p50 and p65/p65 homodimers, ensuring fidelity in NF- κ B signaling.

¹Department of Biochemistry and Molecular Biology, Thomas Jefferson University, 1020 Locust Street, Philadelphia, PA 19107, USA. ²Center of Infectious Disease Research, Walter Reed Army Institute of Research, Silver Spring, MD, USA. ³Macromolecular Diffraction Facility, Cornell High Energy Synchrotron Source (MacCHESS), Cornell University, 161 Synchrotron Drive, Ithaca, NY 14853, USA. ✉email: gino.cingolani@jefferson.edu

The transport of macromolecules into and out of the cell nucleus is essential for cell physiology and is increasingly linked to the degenerative processes that lead to human diseases. The nuclear pore complex (NPC), the only gateway connecting the cytoplasm and nucleoplasm, functions as a semi-permeable barrier. While smaller molecules (<40 kDa) can diffuse through the NPC passively, most macromolecules in a cell, regardless of their size, shuttle through the NPC via an energy-dependent active transport^{1–3}. Cytoplasmic cargos targeted for active nuclear import expose a nuclear localization sequence (NLS) recognized by soluble transport receptors. Several pathways for nuclear import have been described, which share similar principles and rely on soluble transport factors of the importin β superfamily (or β -karyopherins)⁴. These macromolecules promote active, signal-mediated nuclear translocation of cargos by coordinating three activities: high-affinity binding to the NLS-cargo; high-avidity association with the phenylalanine-glycine (FG) repeats lining the inner part of the NPC⁵; and, in the nucleus, binding to the small GTPase RanGTP, which promotes dissociation from FG-nups and NLS-cargo release.

Importin β can import NLS-cargos directly by either binding to their exposed NLSs⁶ or through specialized adaptor proteins such as snurportin and importin α ⁷. In the classical pathway, importin α binds to importin β through its N-terminal Importin- β binding (IBB) domain^{8,9} and to NLS-cargos through its C-terminal 10 stacked Armadillo motifs (Arms) that collectively form an Arm-core^{10,11}. Importin α possesses two NLS binding pockets located along the concave Arm-core surface: an N-terminal ‘major site’ and C-terminal ‘minor site’ between Arms 2–4 and 6–8, respectively^{10,11}. There are seven genes for importin α in the human genome, classified into three clades, with importin $\alpha 1$ presumably functioning as the generic adapter for NLS cargoes⁷. Importin $\alpha 1$, and to some extent other isoforms⁷, is auto-inhibited by the IBB domain that folds back on itself, occupying both NLS sites¹¹. In the presence of importin β and NLS-cargo, the IBB domain is displaced, and the NLS binding sites become accessible for NLS cargo recognition^{8,11}. A plethora of crystal structures has elucidated the recognition of NLS peptides by importin α ¹². The classical monopartite NLS, exemplified by the SV40 T-large antigen NLS, contains a short stretch of basic residues (KKKRRK) that binds primarily to the major NLS binding site and, to a lesser extent, the minor site¹⁰. The bipartite nucleoplasmin NLS (KR-X₁₀-KKKK)¹², on the other hand, contains two clusters of basic residues separated by 10–12 residues, which span both NLS-binding sites. Also, several monopartite NLSs bind selectively to either the major^{13,14} or minor NLS site^{8,15–17}, and their interaction can be regulated by phosphorylation¹⁸. Recent work has revealed that importin α isoforms recognize certain NLS-cargos with a great deal of specificity. For instance, importin $\alpha 3$ selectively imports NF- κ B p50/p65^{19,20} and RCC1²¹. Likewise, viruses infecting human cells hijack specific isoforms, as shown for HIV-1 INV^{22,23}, influenza PB2²⁷, and Nipah and Hendra virus W protein²⁴ that are specific for importin $\alpha 3$ while influenza NP²⁵ and STAT1^{26,27} appear to use importin $\alpha 5$. Overall, selective recognition of NLS-cargos by importin α isoforms is likely to play a role in cellular differentiation^{28,29} and disease states, including viral infections, cancer⁷, and developmental defects^{28,30}.

The nuclear factor-kappa B (NF- κ B) family consists of essential transcription factors mediating various cellular processes, including immune response, cellular differentiation, and apoptosis^{31–33}. There are five known NF- κ B subunits; p65 (RelA), RelB, cRel, and the precursors p105 and p100, which are partially digested to form the p50 and p52 subunits, respectively³¹. These NF- κ B subunits exist as a variety of homodimers and heterodimers, of which p50/p65 represents the most abundant and

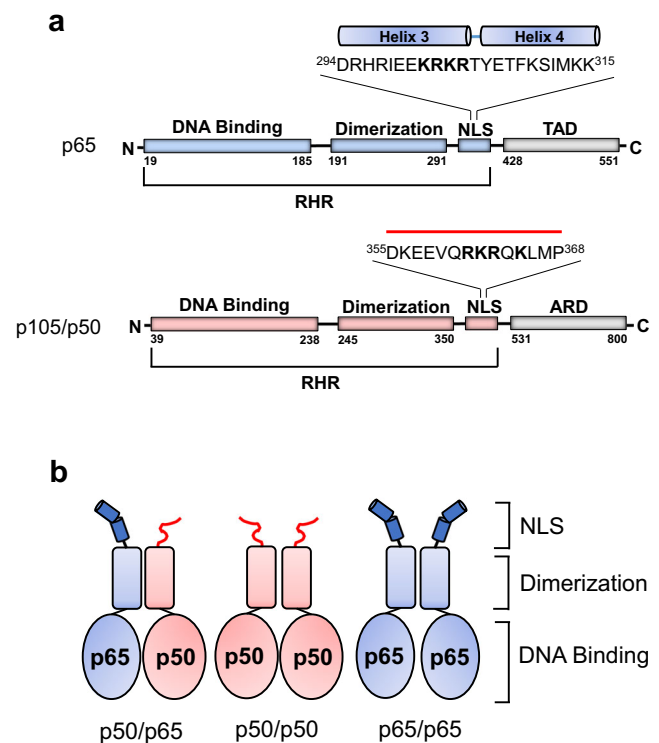


Fig. 1 Topology of NF- κ B p65 and p50. **a** A schematic diagram of the p65 and p50 subunits with the position and sequence of the functional NLSs highlighted. The α -helices in the p65-NLS are based on the crystal structure of p65 bound to I κ B α (PDB: 1IKN). **b** Cartoon of the NF- κ B complexes with the p50- and p65-NLSs colored in red and blue, respectively.

signaling active species³¹. Overall, all NF- κ B subunits contain an N-terminal Rel homology region (RHR) responsible for DNA binding, dimerization, and nuclear localization (Fig. 1a, Supplementary Fig. 1a). In contrast, only the p65, RelB, and cRel contain a C-terminal transactivation domain (TAD) responsible for gene expression³¹. The NF- κ B complexes can signal through either the canonical or non-canonical (alternative) pathway, and specific NF- κ B subunits regulate each pathway. In the canonical NF- κ B signaling pathway, a diverse subset of stimuli, including inflammatory cytokines and chemokines, activates the p65, p50, and cRel subunits and triggers rapid and transient NF- κ B response³⁴. The non-canonical NF- κ B pathway, on the other hand, is triggered by a smaller subset of stimuli, which activates RelB and p52 and leads to long-term, persistent NF- κ B signaling³⁵. The p50/p65 heterodimer, the most abundant signaling complex in the canonical NF- κ B pathway, is expressed in all cell types, while the p65/p65 and p50/p50 homodimers are less abundant^{31,36}. The p50/p65 cellular abundance reflects the greater structural stability of the NF- κ B heterodimer compared to homodimers³⁶. The p50/p65 dimerization interface is stabilized by a network of hydrogen bonds and salt bridges, including an energetically favorable interaction between Asp254 from p50 and the equivalently positioned Asn200 in p65^{37,38}, which is missing in the p50/p50 and p65/p65 homodimers. Comparing homodimers stability, Tyr267 and Phe307 in p50 are replaced by Phe213 and Val248 in p65, respectively, which reduce both the H-bonding and hydrophobic interactions stabilizing the p65 homodimer^{36,39,40}. Thus, the NF- κ B p50/p65 is more stable than p50/p50, and the p65/p65 homodimer is the least stable of the three NF- κ B dimers.

The nuclear translocation of NF- κ B species is tightly regulated in human cells. Fagerlund et al.^{19,20} identified a functional NLS

responsible for nuclear import at the C-termini of p50 and p65 RHR (Fig. 1a, b). In the canonical NF- κ B signaling pathway, the NF- κ B p50/p65 and p65/p65 complexes are regulated by binding to the Inhibitor of NF- κ B (I κ B) proteins, which retain the complex in the cytoplasm and mask the p65-NLS^{41,42}. Meanwhile, the p50 precursor p105, which lacks a TAD domain, possesses a C-terminal Ankyrin-like repeating domain (ARD) which mimics I κ B and retains the precursor p105/p50 complex in the cytoplasm⁴³. In the resting state, the NF- κ B complex is sequestered in the cytoplasm either by I κ B α -mediated retention for the p50/p65 and p65/p65 complexes⁴⁴ or ARD-mediated retention for the precursor p105/p50 complex^{45,46}. Upon stimulation, the activated inhibitor of NF- κ B kinase complex (NEMO/IKK β /IKK α)^{31,47} promotes I κ B phosphorylation, ubiquitination, and the eventual dissociation and proteasomal degradation^{48,49}, which removes the I κ B repression from p50/p65 and p65/p65 complexes. The newly liberated NF- κ B p50/p65 complex is then shuttled into the nucleus by the isoforms importin α 3 and α 4, which are 95% identical in sequence^{19,20}. The p65/p65 homodimer can also localize to the nucleus by binding to importin α 3 and α 4 as well as other isoforms, including importin α 1 and importin α 8^{19,20,50,51}. Similarly, for the p105/p50 complex, the activated IKK-mediated signaling leads to ARD cleavage by the 20S proteasome and liberation of the p50/p50 homodimer that exposes the NLSs for importin α 3/ α 4-mediated nuclear import^{19,20,52}. Overall, the exact mechanisms of NF- κ B homodimers (p50/p50 and p65/p65) nuclear import have not been elucidated. In vitro transfection studies of p65 and p50^{19,20} could not fully distinguish between the heterodimeric p50/p65, the most abundant NF- κ B species in human cells, and the less abundant homodimeric complexes formed by p50/p50 and p65/p65.

Here, we have investigated how NF- κ B complexes interact and discriminate between importin α isoforms. Using hybrid

structural methods, we found that the p50-NLS and the p65-NLS bind different regions of importin α 3, generating a trans bipartite NLS. Unexpectedly, the two NLSs reveal surprising structural polymorphisms in the context of different NF- κ B dimers.

Results

Stoichiometry of the canonical NF- κ B p50/p65 nuclear import complex. To shed light on the NF- κ B nuclear import complexes' composition and structure, we purified NF- κ B subunits p50 and p65 RHR, including the C-terminal NLS. Removing the TAD does not affect dimerization that is solely dictated by the dimerization domain^{37,38,41,42}. We assembled and purified three NF- κ B dimers (Fig. 1b, Supplementary Fig. 1b) and human importin α 1 and α 3 lacking the autoinhibitory N-terminal IBB domain¹¹ (Δ IBB-importin α 1 and α 3). To elucidate the association of either importin α isoform with p50/p65, we added an increasing molar excess of purified p50/p65 to 10 μ g of purified Δ IBB-importin α 1 (Fig. 2a) or α 3 (Fig. 2b) and analyzed the resulting mixture by native gel electrophoresis. We found that only one equivalent of p50/p65 heterodimer was sufficient to entirely shift the migration of either importin α isoform, suggesting a 1:1:1 stoichiometry between Δ IBB-importin α , p50, and p65 (red star in Fig. 2a, b). We confirmed this stoichiometry using a p50/p65 heterodimer that contains a shorter version of p50 lacking the DNA-binding domain Δ DBD-p50, also competent for heterodimerization with p65⁴¹. The smaller Δ DBD-p50/p65 heterodimer bound one equivalent of Δ IBB-importin α 3, eluting as a monodisperse 1:1:1 species by SEC (Fig. 2c). This complex was comparatively larger than Δ DBD-p50/p65 complex but similar to Δ IBB-importin α 3 alone, which is elongated and can dimerize in solution⁵³. The eluted complex contained three stoichiometric bands for p65, Δ DBD-p50, and Δ IBB-importin α 3

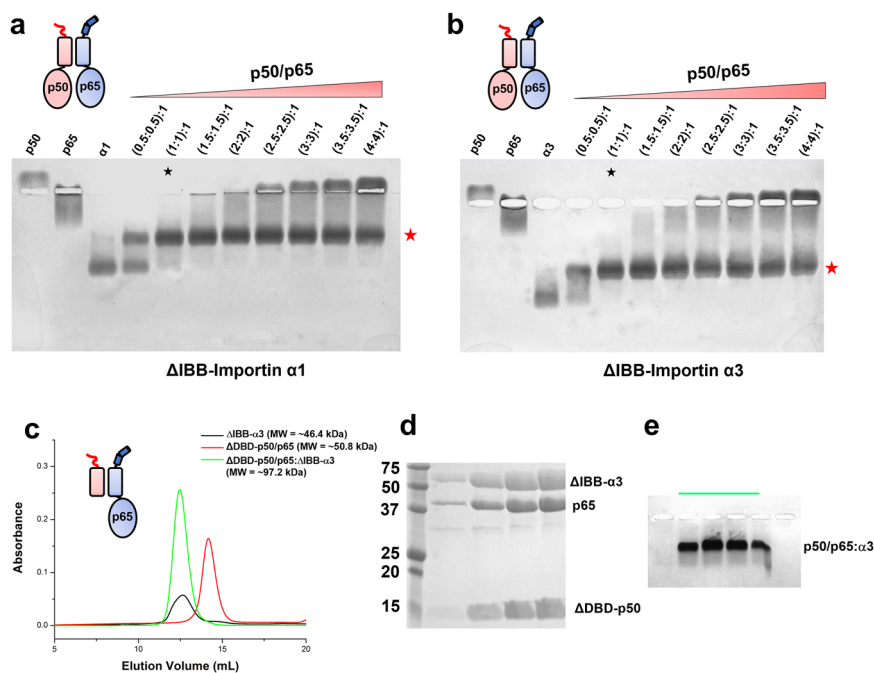


Fig. 2 Stoichiometric binding of importin α 3 to the NF- κ B p50/p65 heterodimer. Native agarose gel electrophoresis on agarose showing a titration of purified p50/p65 complex against a fixed 10 μ g (~108 pmoles) of Δ IBB-importin α 1 (**a**) and α 3 (**b**). The p50/p65: Δ IBB-importin titration is labeled as an (X:X):1 molar ratio where (X:X) corresponds to the moles of p50 and p65 subunits. The red star denotes the p50/p65: Δ IBB-importin α complex in a stoichiometric 1:1:1 ratio. Data are representative of two independent experiments. Source data are provided as a Source Data file. **c** SEC assembly of the NF- κ B trimeric p50/p65- Δ DBD- Δ IBB-importin α 3 import complex (green line) from purified Δ IBB-importin α 3 (gray line) and Δ DBD-p50/p65 complex (red line). The peak fraction from panel **c** was analyzed by SDS-PAGE (**d**) and on a native agarose gel (**e**). The data shown in panels **d** and **e** are representative of two independent experiments. Source data are provided as a Source Data file.

when analyzed by SDS-PAGE (Fig. 2d), but only one slowly moving species by native gel electrophoresis (Fig. 2e), indicative of a stable molecular complex. Thus, both importin $\alpha 1$ and $\alpha 3$ can bind the p50/p65 in vitro with a 1:1:1 stoichiometry, although isoform $\alpha 3$ is the preferred isoform in a cell^{19,20}.

The p50-NLS in p50/p65 is the dominant binding determinant for importin $\alpha 3$. To determine how the p65- and p50-NLSs mediate binding to importin α , we generated constructs of p65 and p50 lacking the C-terminal NLS and assembled all possible permutations of dimeric NF- κ B complexes (Supplementary Fig. 1b). Using an ELISA-based microtiter binding assay, we systematically compared the binding of Δ IBB-importin $\alpha 3$ for NF- κ B dimers containing two NLSs (p50/p65; p65/p65; p50/p50), only one NLS (Δ NLS-p50/p65, Δ NLS-p50/p65) or lacking the NLSs (Δ NLS-p50/ Δ NLS-p65, Δ NLS-p65/ Δ NLS-p65, Δ NLS-p50/ Δ NLS-p50) (Fig. 3). Given the number of different NF- κ B constructs to analyze (Supplementary Fig. 1b), we performed two sets of experiments. In the first set, we compared the binding of Δ IBB-importin $\alpha 3$ to four permutations of the heterodimeric p50/p65 (Fig. 3a). We found that Δ IBB-importin $\alpha 3$ bound the p50/p65 heterodimer with an equilibrium binding constant of $K_D = 45.8 \pm 0.9$ nM. Deleting the p50-NLS abolished association with Δ IBB-importin $\alpha 3$, while the p50/ Δ NLS-p65 was just as potent as the wild-type NF- κ B ($K_D = 59.6 \pm 2.2$ nM) though had a slightly decreased number of binding sites at equilibrium (Bmax).

In the second set of experiments (Fig. 3b), Δ IBB-importin $\alpha 3$ was titrated against plates pre-activated with p50/p50 or p65/p65 homodimers. This assay revealed that Δ IBB-importin $\alpha 3$ bound p50/p50 and p65/p65 with $K_D = 15.4 \pm 0.2$ and 35.2 ± 0.9 nM, respectively. Interestingly, the p50/p50 homodimer had a Bmax

twice as large as the p65/p65, suggesting a double number of Δ IBB-importin $\alpha 3$ bound the p50/p50 at equilibrium compared to p65/p65. Removing the NLS from either homodimer completely obliterated binding to Δ IBB-importin $\alpha 3$, suggesting the p65- and p50-NLSs are the major binding determinants in the context of NF- κ B homodimers. To confirm the nanomolar affinities observed in vitro, both p50 and p65 dimerization domains were co-expressed in bacteria with Δ IBB-importin $\alpha 3$ and found to assemble into stable complexes that could be readily isolated by SEC (Supplementary Fig. 2a, b). Thus, the p50-NLS appears to be the dominant NLS in the context of the NF- κ B p50/p65 heterodimer, while individual p50- and p65-NLSs are sufficient for high-affinity binding of NF- κ B homodimers to importin $\alpha 3$.

Competition between I κ B α and importin $\alpha 3$. The inhibitor I κ B α binds a region of NF- κ B encompassing the p65-NLS but does not contact the p50-NLS that remains solvent-exposed in the crystal structure^{41,42}. Next, we explored the competition between I κ B α and importin $\alpha 3$ for binding to NF- κ B p50/p65. We purified recombinant I κ B α and titrated the purified protein against a pre-formed NF- κ B p50/p65 heterodimer. The resulting complex was visualized using a native agarose gel (Fig. 4a). In agreement with the literature^{41,42}, I κ B α bound the p50/p65 stoichiometrically in a 1:1:1 molar ratio (Fig. 4a, lane 5), corresponding to one equivalent of I κ B α per p50/p65 heterodimer. Excess I κ B α was readily visible at the bottom of the gel, migrating as a band with faster mobility (Fig. 4a, lane 6–10). Next, we titrated increasing I κ B α against a pre-formed p50/p65: $\alpha 3$ complex formed using a 1:1:1 ratio of the three proteins (see the control in Fig. 4a, lane 3). Even at the lowest I κ B α concentration (Fig. 4a, lane 11), all importin $\alpha 3$ was

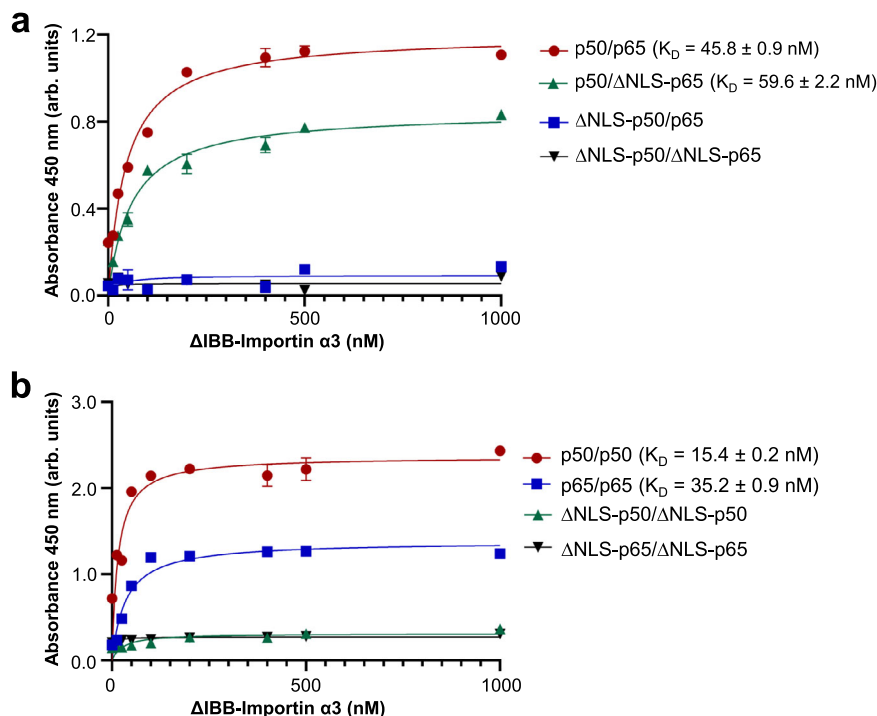


Fig. 3 ELISA-based microtiter binding assays. **a** Δ IBB-importin $\alpha 3$ was titrated against p50/p65 (red), p50/ Δ NLS-p65 (green), p50- Δ NLS/p65 (blue), Δ NLS-p50/ Δ NLS-p65 (black). The dissociation constant (K_D) of Δ IBB-importin $\alpha 3$ for p50/p65 and Δ NLS-p50/p65 is $K_D = 45.8 \pm 0.9$ and 59.6 ± 2.2 nM, respectively. Non-saturable binding was observed for Δ NLS-p50/p65 and Δ NLS-p50/ Δ NLS-p65. **b** Δ IBB-importin $\alpha 3$ was titrated against p50/p50 (red), p65/p65 (blue), Δ NLS-p50/ Δ NLS-p50 (green), and Δ NLS-p65/ Δ NLS-p65 (black). The dissociation constant (K_D) of Δ IBB-importin $\alpha 3$ for p50/p50 and p65/p65 is $K_D = 15.4 \pm 0.2$ and 35.2 ± 0.9 nM, respectively. No measurable binding was observed for Δ NLS-p65/ Δ NLS-p65 and Δ NLS-p50/ Δ NLS-p50. The standard deviation was calculated from averaging two independent experiments. Source data are provided as a Source Data file.

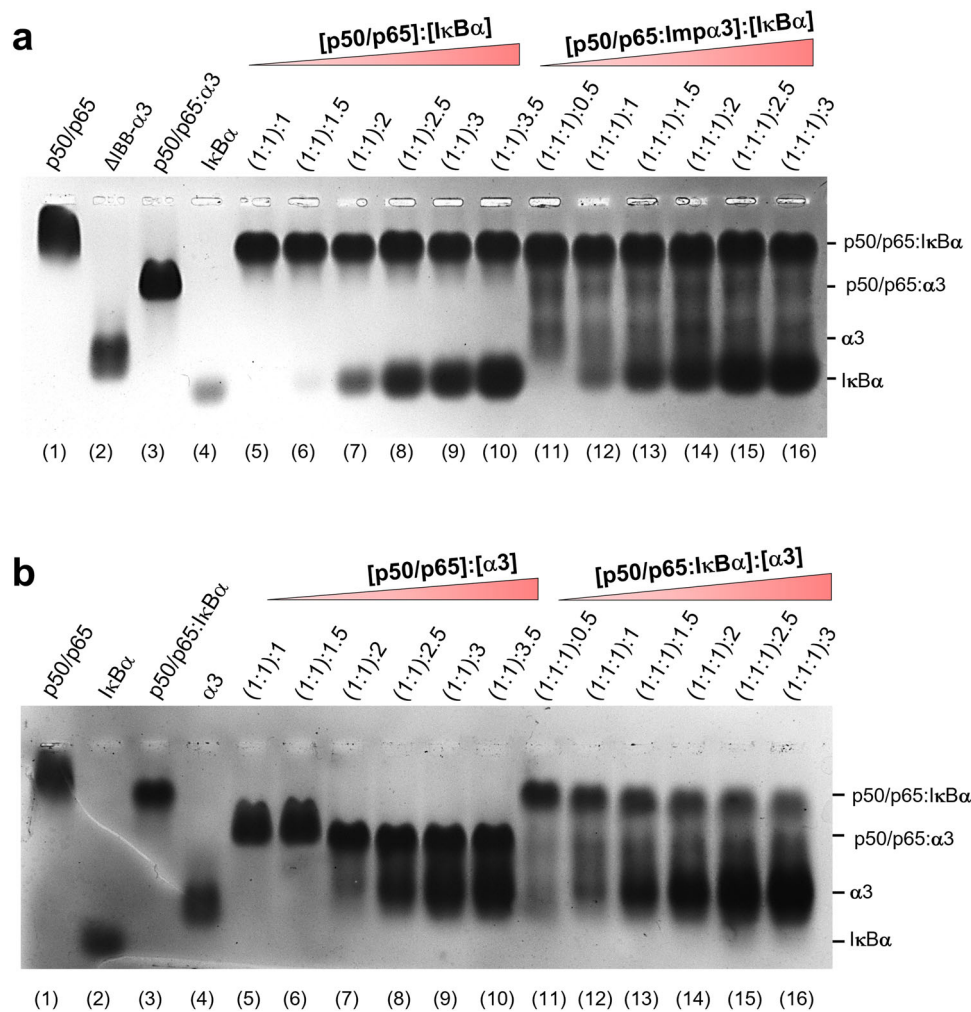


Fig. 4 Competition between IκBα and ΔIBB-importin α3 for NF-κB p50/p65. **a** Native agarose gel electrophoresis showing a titration of purified IκBα against ~130 pmoles of pre-formed p50/p65 (lanes 5–10) or p50/p65:ΔIBB-importin α3 complex (lanes 11–16). The moles of IκBα are relative to those of individual species in pre-formed dimeric and trimeric complexes. All controls in lanes 1–4. **b** Native agarose gel electrophoresis showing a titration of purified ΔIBB-importin α3 against ~130 pmoles of pre-formed p50/p65 (lanes 5–10) or p50/p65:IκBα (lanes 11–16). The moles of ΔIBB-importin α3 are relative to those of individual species in pre-formed dimeric and trimeric complexes. The data shown in panels **a** and **b** are representative of two independent experiments. Source data are provided as a Source Data file.

displaced from p50/p65, giving rise to the p50/p65:IκBα complex (Fig. 4a, lanes 11–16). We also performed a converse experiment whereby a stoichiometric p50/p65:IκBα complex was first formed using a 1:1:1 molar ratio of p50/p65 and IκBα (Fig. 4b, lane 3), and then challenged with an increasing molar excess of purified importin α3 (Fig. 4b, lane 11–16). Even at a super-physiological importin α3 concentration of ~54 μM, over 50× higher than the estimated cellular concentration for all isoforms⁵⁴, the inhibited p50/p65:IκBα complex remained intact, and there was no appearance of the p50/p65:α3 complex on the gel (shown in Fig. 4b, lane 5). Overall, these data suggest that IκBα and importin α3 binding to p50/p65 are mutually exclusive. Though exposed in the trimeric p50/p65:IκBα complex^{41,42}, the p50-NLS is not accessible for association with importin α3 when IκBα is present.

Crystallographic analysis of importin α isoforms 1 and 3 bound to NF-κB NLSs. To visualize NF-κB's association with importins, we attempted crystallization of the p50/p65 heterodimer in complex with importin α isoforms but were unsuccessful. Large crystals of the NF-κB p50/p50 homodimer were obtained with ΔIBB-importin α3 but failed to diffract X-ray

beyond 10 Å resolution. We then turned to study the structure of importin α isoforms 1 and 3 in complex with p50- and p65-NLS peptides (Fig. 1a). In total, we obtained and solved five crystal structures (Table 1): two complexes of human ΔIBB-importin α3, either bound to the p50-NLS alone or both p65- and p50-NLS peptides (Fig. 5a, b), and three complexes of the mammalian ΔIBB-importin α1 bound to p65-NLS or p50-NLS alone, as well as both p65- and p50-NLS peptides (Fig. 5d–f). The best importin α3 crystals diffracted to 2.10 Å for the p50-NLS complex and 2.85 Å with p65/p50-NLS peptides. Similarly, the best diffraction data for importin α1 (~2.20 Å) were obtained from crystals bound to just the p50-NLS, while a complex with both the p65/p50-NLSs or just the p65-NLS diffracted to 2.40 and 2.82 Å resolution, respectively (Table 1). Molecular replacement for the NF-κB NLS/importin α3 complexes was initially attempted using the apo importin α3 structure²⁴ as a search model but yielded a poor solution with a high clash score. In contrast, the Nipah virus W protein-bound importin α3 structure²⁴ yielded a straightforward solution, which could be easily refined to an Rfree under 30%. All crystal structures had clear electron densities for the p50- and p65-NLSs and adjacent flanking regions that we modeled in unbiased $F_0 - F_c$ electron density maps and confirmed in Polder

Table 1 Crystallographic data collection and refinement statistics.

	Δ IBB-imp $\alpha 3$ + p50-NLS	Δ IBB-imp $\alpha 3$ + p50-NLS + p65-NLS	Δ IBB-imp $\alpha 1$ + p65-NLS	Δ IBB-imp $\alpha 1$ + p50-NLS	Δ IBB-imp $\alpha 1$ + p50-NLS + p65-NLS
<i>Data collection</i>					
Beamline	SSRL 12-1	SSRL 12-1	SSRL 9-2	SSRL 12-1	SSRL 12-1
Wavelength (Å)	0.953	0.979	0.979	0.979	0.979
Space group	P2 ₁	P3 ₂ 2 ₁	P2 ₁ 2 ₁ 2 ₁	P2 ₁ 2 ₁ 2 ₁	P2 ₁ 2 ₁ 2 ₁
Cell dimensions <i>a</i> , <i>b</i> , <i>c</i> (Å)	47.6, 59.0, 86.0	117.1, 117.1, 210.2	78.5, 90.8, 99.8	78.1, 90.7, 97.4	77.9, 91.2, 97.2
α , β , γ (°)	90.0, 96.3, 90.0	90.0, 90.0, 120.0	90.0, 90.0, 90.0	90.0, 90.0, 90.0	90.0, 90.0, 90.0
Reflections (tot/unique)	1,021,555/27,642	471,279/34,874	665,708/17,271	768,008/27,626	370,915/24,702
Resolution (Å)	30.0–2.10 (2.16–2.10)	50.0–2.82 (2.92–2.82)	15.0–2.81 (2.91–2.81)	15.0–2.24 (2.33–2.24)	50.0–2.40 (2.49–2.40)
Completeness (%)	98.8 (87.7)	85.4 (45.5)	97.7 (89.3)	81.9 (87.1)	89.2 (57.8)
Redundancy	5.5 (4.3)	3.1 (2.9)	6.9 (4.6)	3.8 (3.0)	3.1 (2.2)
<i>R</i> _{sym}	6.4 (55.2)	13.7 (85.3)	11.1 (53.0)	9.1 (85.2)	12.4 (81.6)
<i>R</i> _{pim}	4.4 (41.2)	8.2 (71.2)	7.3 (73.0)	7.7 (74.8)	8.0 (70.8)
<i>I</i> / σ ₁	11.6 (2.4)	6.3 (1.2)	14.5 (1.5)	14.4 (1.5)	13.2 (1.2)
CC1/2	0.998 (0.815)	0.994 (0.287)	0.995 (0.718)	0.996 (0.309)	0.988 (0.409)
Wilson B-factor (Å ²)	42.0	64.1	70.1	38.2	51.6
<i>Refinement</i>					
PDB entry	7LFC	7LF4	7LEU	7LEQ	7LET
Resolution limits (Å)	15.0–2.10	15.0–2.85	15–2.82	15–2.24	50–2.40
No. of reflections	27,534	25,877 ^a	17,116	27,564	24,529
<i>R</i> _{work} / <i>R</i> _{free} ^b	19.9/22.0	19.6/23.7	20.0/23.5	19.1/21.8	19.8/24.1
No. of copies Asym. Unit	1	2	1	1	1
No. of protein atoms	3302	6859	3361	3291	3358
No. of solvent	105	0	1	149	32
Ramachandran (%) allow/gener/ disallowed Rms from ideal	98.34/1.66/0.0	96.20/3.80/0.0	97.22/2.78/0.0	98.12/1.88/0.0	97.44/2.56/0.0
Bond lengths (Å)	0.009	0.005	0.007	0.006	0.006
Bond angles (°)	1.06	1.08	1.05	1.09	0.82
MolProbity Score	1.38	1.87	1.52	1.45	1.41
MolProbity Clashscore	6.33	12.6	6.76	8.39	6.17

Values in parentheses are for the highest-resolution shell.
^aReflections with $|F_{obs}|/\sigma F_{obs} > 2.15$.
^bThe *R*_{free} value was calculated using 5% of randomly selected reflections.

maps (Supplementary Figs. 3 and 4). The final models have *R*_{free} under 24% and excellent stereochemistry (Table 1), allowing for a direct structural comparison of the five crystallographic structures.

The p50-NLS binds exclusively to the major NLS-binding pocket. Both Δ IBB-importin $\alpha 3$ and $\alpha 1$ crystallized with an excess of the p50-NLS had strong electron density for the NLS only at the major NLS binding site (Supplementary Figs. 3a and 4a). The two isoforms adopt a nearly identical conformation of the Arm core, and the p50-NLS P₁–P₅ residues (Arg361–Lys365) are not only superimposable in the two complexes (RMSD of 1.095) (Fig. 6a) but also occupy equivalent positions. However, the p50-NLS binds more intimately with importin $\alpha 3$ than $\alpha 1$, contributing 18 hydrogen bonds, two salt bridges, 152 Van der Waals contacts, and burying a surface area of 855.8 Å² (Fig. 6c) versus nine hydrogen bonds, no salt bridges, 118 Van der Waals contacts, and burying a surface area of only 780.4 Å² in $\alpha 1$ (Fig. 6e). Accordingly, eleven residues of the p50-NLS (res. 358–368) were modeled in the importin $\alpha 3$ structure versus only seven (res. 361–367) for importin $\alpha 1$. In both complexes, the p50-NLS residues ³⁶¹RKRQK³⁶⁵ occupy the P₁–P₅ positions at the major NLS-binding pocket (Supplementary Table 2), with Lys362 at the crucial P₂ position. Additionally, the p50-NLS contains an N-terminal extension ³⁵⁶KEEVQ³⁶⁰ immediately upstream of the NLS that bears a considerable amount of negatively charged residues, including Glu357, which makes a salt bridge with importin $\alpha 3$ Arg306 in the importin $\alpha 3$ + p50-NLS complex

(Fig. 6c). Comparing the p50-NLS sequence to the NLSs of hPLSCR1, Ku70, and Ku80, which also binds only at the major NLS site^{13,14}, reveals conservation of a Lys at the P₅ site (Supplementary Table 2) that makes hydrogen bonds with Gln176 and Asn141, possibly explaining why the p50-NLS targets the major NLS-binding pocket only. Thus, the crystallographic analysis of importin $\alpha 1$ and $\alpha 3$ bound to the p50-NLS reveals this NLS binds exclusively to the major NLS-binding pocket, explaining the specificity for the isoform $\alpha 3$ reported in the literature¹⁹.

The p65-NLS binds differently to the major and minor NLS-pockets. Only the isoform $\alpha 1$ crystallized bound to the p65-NLS alone. A 2.8 Å crystal structure revealed two p65-NLS peptides bound to the major and minor NLS pockets (Fig. 5e, Supplementary Fig. 4b) in slightly different conformations. At the major site (Fig. 6g), the p65-NLS occupies sites P₁–P₅ in a p50-NLS-like conformation, with Glu300, Lys301, Arg302, Lys303, and Arg304, making a total of 11 hydrogen bonds, 101 Van der Waals contacts, and burying 724.2 Å². Unlike the p50-NLS, which inserts Arg361 into the P₁ position and is stabilized by Van der Waals interactions, the Glu300 in the p65-NLS orients away from the P₁ position (Fig. 6g). The p65-NLS also occupies the minor NLS pocket (Fig. 6h). This binding includes ten hydrogen bonds and 88 Van der Waals contacts but no salt bridges, with the Arg302 occupying the P₂' position (Supplementary Table 2).

Interestingly, adding both p65- and p50-NLS peptides to importin $\alpha 3$ (Fig. 5b) and $\alpha 1$ (Fig. 5f) resulted in strong electron density for the p65-NLS peptide at the minor site, with the

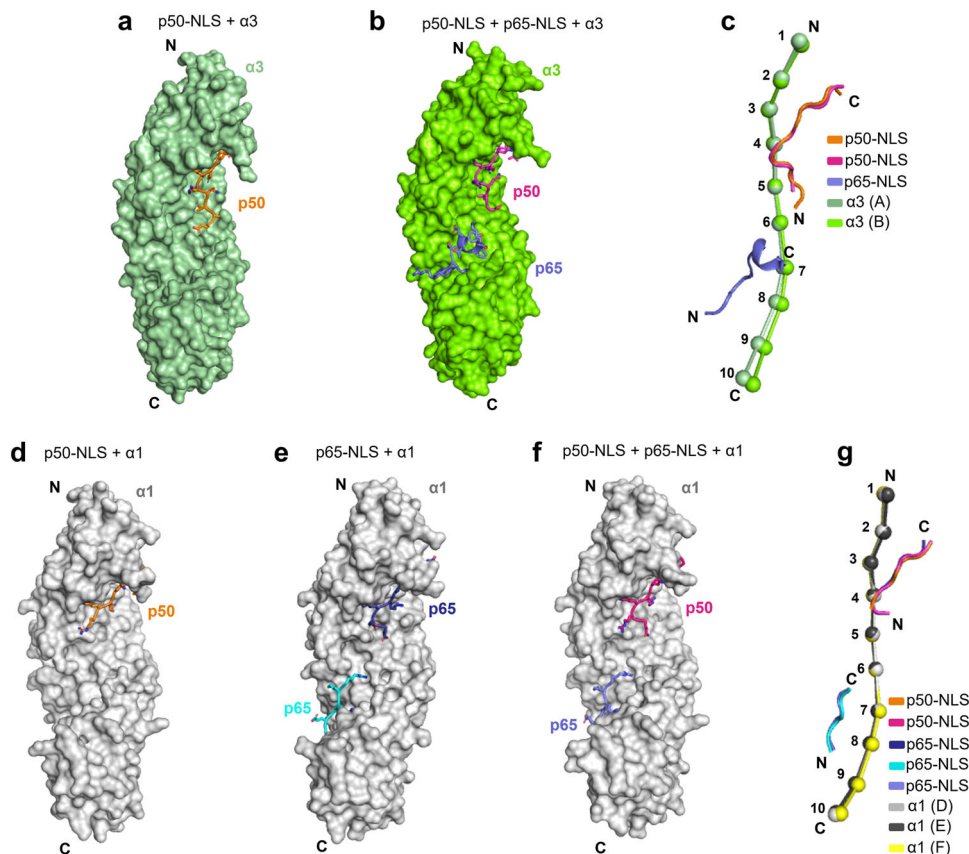


Fig. 5 Crystal structures of Δ IBB-importin $\alpha 3$ and $\alpha 1$ bound to NF- κ B p65- and p50-NLS peptides. Surface representation of Δ IBB-importin $\alpha 3$ (colored in dark and light green) bound to the (a) p50-NLS (orange) (b) p50- and p65-NLSs (magenta and blue), respectively. Δ IBB-importin $\alpha 3$ bound to p50- and p65-NLSs crystallized as a dimer, but only one chain (chain C) is shown in panels b, c. The two chains in the asymmetric unit are nearly identical (RMSD = 1.14 Å), but the dimer is likely a crystallographic artifact due to the high concentration used for crystallization. Both importin $\alpha 3$ molecules in the asymmetric unit are bound to the p50- and p65-NLS peptides, which occupy identical binding sites and have similar structures. However, one of the importin $\alpha 3$ molecules (chain A) has a higher B-factor, likely due to weaker crystal contacts, which prompted us to use chain C for structural analysis. c Superimposition of importin $\alpha 3$ structures in A (dark green) and B (light green) shown as beads-on-a-string. Surface representation of Δ IBB-importin $\alpha 1$ (colored in light gray) bound to the (d) p50-NLS (orange), (e) p65-NLS (dark blue and cyan), and (f) p50- and p65-NLSs (magenta and blue). g Superimposition of all importin $\alpha 1$ structures in d (light gray), e (dark gray), and f (yellow) shown as beads-on-a-string.

p50-NLS firmly occupying the major NLS-site (Supplementary Figs. 3b and 4c). However, there were noticeable differences between the p65-NLS conformations and contacts made with either isoform (Fig. 6b). In the importin $\alpha 3$ co-crystal structure with the p65- and p50-NLSs (Fig. 6d), the eleven residue p65-NLS can be divided into two stretches, with the N-terminal residues $^{301}\text{KRKR}^{305}$ adopting an extended conformation and the C-terminal residues $^{306}\text{YETFKS}^{311}$ folding into an α -helix. The residues $^{303}\text{KRKYE}^{307}$ occupy the P_1' - P_5' positions, including the helical conformation contributing to a salt bridge between p65-NLS Glu307 and importin $\alpha 3$ Lys231 within the Arm 4 coiled region (Supplementary Table 2). The p65-NLS helical conformation resembles the p65 helical structure visualized in the I κ B α - and I κ B β -NF- κ B complexes^{41,42} with the helix 4 (res. 305–311) retained and bound to both I κ B α and importin $\alpha 3$. In contrast, the p65-NLS residues 294–303 fold into α -helix (referred to as helix 3) in the I κ B-bound complex but bind importin $\alpha 3$ in an extended conformation. Unexpectedly, in all complexes with importin $\alpha 1$, the p65-NLS adopts a fully extended conformation at the minor NLS-site, with the P_1' - P_4' positions occupied by $^{301}\text{KRKR}^{304}$ residues (Fig. 6f, h); the α -helix $^{306}\text{YETFKS}^{311}$ seen in complex with importin $\alpha 3$ (Fig. 6d) is missing in these structures.

The mechanism by which different isoforms accommodate the p65-NLS at the minor NLS-binding pockets determines the

number and types of contacts made in the two complexes. PISA⁵⁵ revealed the p65-NLS:importin $\alpha 3$ binding ($\Delta G = -0.6$ kcal/mol) is more energetically favorable than the p65-NLS:importin $\alpha 1$ ($\Delta G = 4.9$ kcal/mol), which possibly explains the physiological preference for importin $\alpha 3$. Additionally, comparing the p65-NLS in both importin α isoforms, there appears to be a shift in the NLS register at the P_2' position. In the importin $\alpha 1$ structures (Fig. 6f, h), the P_2' position is occupied by Arg302 while Lys301, Lys303, and Arg304 occupy the P_1' , P_3' , and P_4' , respectively, and the P_5' is unoccupied. In contrast, in complex with importin $\alpha 3$ (Fig. 6d), the P_2' position is occupied by Arg304, with Thr305, Tyr306, and Glu307 at the P_3' - P_5' positions, respectively. The residues responsible for generating this frameshift are the same that form the α -helix ($^{306}\text{YETFKS}^{311}$) observed in the importin $\alpha 3$ /p65-NLS complex and are part of the α -helix 4 (res. 306–321) responsible for binding to I κ B α ^{41,42}.

A conformational change in importin $\alpha 3$ Arm-core upon NF- κ B NLS recognition. We compared the structures of importin $\alpha 3$ crystallized with different p50- and p65-NLS peptides and found importin $\alpha 3$ adopts a significantly different conformation when the p65-NLS is bound at the minor NLS-box (Fig. 5c). Importin $\alpha 3$ flexible solenoid can be rationalized as two arches formed by Arms 1–4 and 7–10 flapping dynamically around a central core

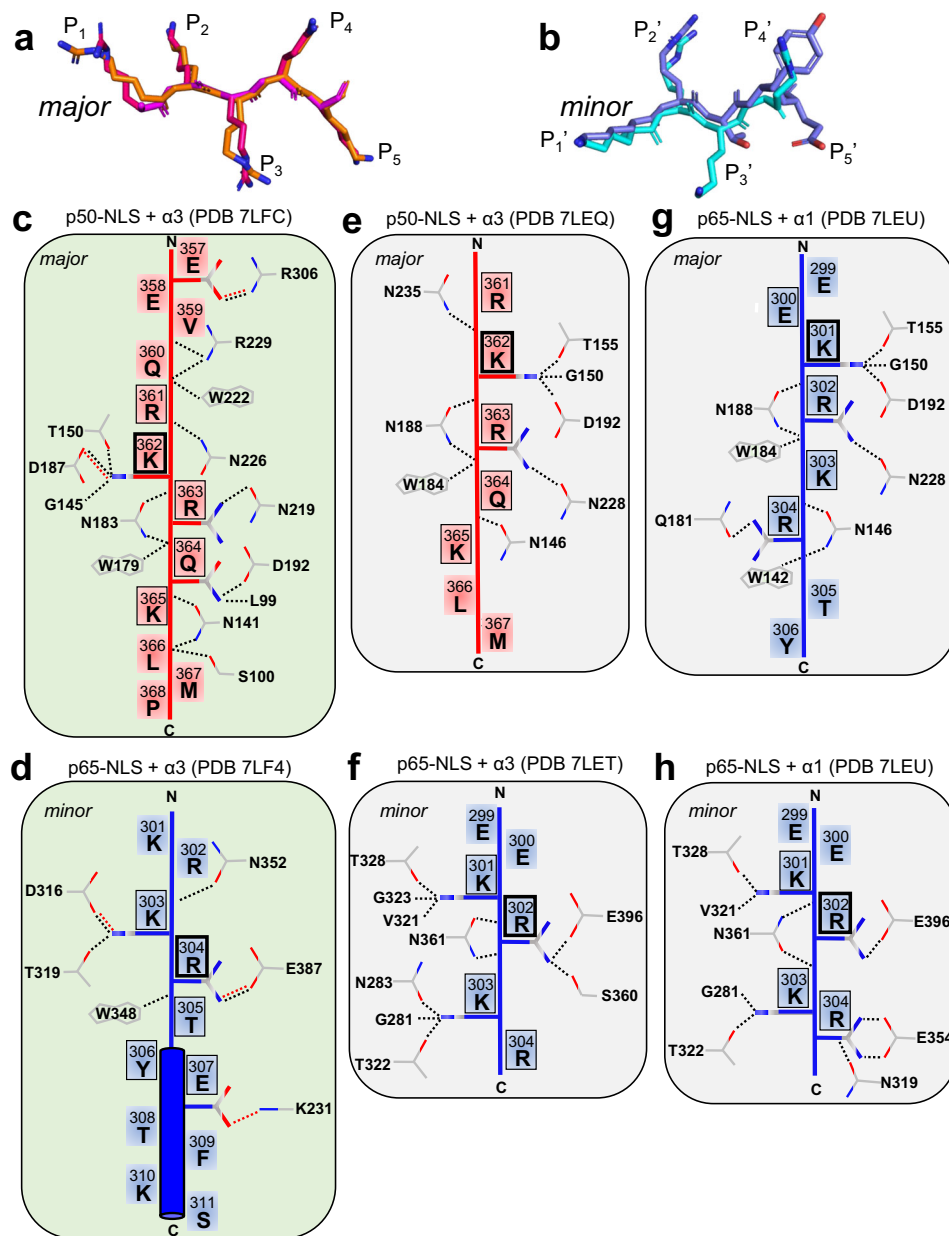


Fig. 6 Schematic of NLS-binding at the major and minor NLS binding site of importin α isoforms. **a, b** Overlay of the p50-NLSs and p65-NLSs P_1 - P_5 positions bound to the major and minor NLS-binding sites of Δ 1BB-importin $\alpha 1$ (orange and cyan, respectively) and $\alpha 3$ (magenta and blue, respectively). **c-h** Schematic diagram of all major contacts made by the p50-NLS (red) and p65-NLS (blue) with Δ 1BB-importin $\alpha 3$ and $\alpha 1$, at the major (panels **c, e, g**) and minor (panels **d, f, h**) NLS-binding sites. All contacts shown occur within 3.5 Å distance: hydrogen bonds and salt bridge interactions are shown by dash lines colored in black and red, respectively. NLS residues occupying positions P_1 - P_5 and P_1' - P_5' are marked with a black frame (thicker for positions P_2 and P_2').

consisting of Arms 5-6⁸. DynDom analysis⁵⁶ of the importin $\alpha 3$ crystal structures in the unliganded state and bound to p50-NLS and p65-/p50-NLSs revealed two structural changes in the peripheral arches in response to the p65-NLS binding. At the N-terminus, a hinge movement⁵⁷ was identified within Arm 4 (res. 198-201) in response to p50-NLS and p50-/p65-NLS binding compared to the apo structure (Supplementary Fig. 5a, b). This hinge movement makes the major site more accessible for the p50-NLS and facilitates numerous intimate p50-NLS contacts. Similarly, DynDom revealed a shear movement within Arm 7 residues 337-338 only in the importin $\alpha 3$ structure with p65-/p50-NLSs (Supplementary Fig. 5b, c). This shear movement, described as a movement along the plane of an interface⁵⁷, exposes an additional ~93 Å surface area and shifts the C-terminal Arm 10 by ~3.5 Å

compared to the apo importin $\alpha 3$ structure. These conformational changes facilitate the closure of the C-terminal arch around the p65-NLS, while Arms 2-4 cradles the p50-NLS peptide. Overall, the segmented motion of importin $\alpha 3$ Arm core allows the minor site to become more accessible, accommodating the partially helical p65-NLS, as previously reported for other $\alpha 3$ -specific NLS-cargos^{24,58}.

SuperPose⁵⁹ revealed importin $\alpha 3$ bound to the p50- and p65-NLSs aligns well at both major and minor NLS sites with the structure of importin $\alpha 3$ bound to SOX2⁵⁸ (RMSD 1.54 Å between residues 72 and 486) (Supplementary Fig. 6). However, the structure of p50/p65: $\alpha 3$ differs significantly from the RCC1-bound importin $\alpha 3$ ²¹ (RMSD 2.00 Å between residues 72-487) and even more from the apo $\alpha 3$ ²⁴ (RMSD 2.80 Å between

residues 72 and 486). Meanwhile, importin $\alpha 1$ residues 75–497 are perfectly superimposable (RMSD 0.26–0.39 Å) in all complexes of importin $\alpha 1$ bound to either p65-, p50-, and both NLSs (Fig. 5g), underscoring the rigid structure of this isoform⁷ that can stretch NLS peptides at the major and minor binding sites by making extensive mainchain contacts. Thus, the intrinsic plasticity of importin $\alpha 3$ appears to play a role in NLS-cargo specificity in contrast to the more rigid importin $\alpha 1$.

Solution structure of NF- κ B p50/p65 bound to importin $\alpha 3$. To investigate the quaternary structure of different NF- κ B import complexes, we performed size-exclusion chromatography coupled with small-angle X-ray scattering (SEC-SAXS)⁶⁰. A pre-assembled complex of NF- κ B p50/p65 (Fig. 7a) bound to Δ IBB-importin $\alpha 3$ was analyzed on an analytical Superdex gel filtration column and eluted fractions were subjected to SAXS using a 0.25 mm \times 0.25 mm microbeam. The resulting SEC-SAXS profiles were proven suitable for biophysical analysis. We found the p50/p65: Δ IBB-importin $\alpha 3$ complex has a radius of gyration (R_g) of 44.21 ± 0.28 Å (Fig. 7a, Supplementary Table 3), and a volume of correlation⁶¹ mass of 124.4 ± 12.4 kDa, in close agreement with the theoretical MW ~ 129 kDa expected for a heterotrimer of p50/p65: Δ IBB-importin $\alpha 3$ in a 1:1:1 stoichiometry (Supplementary Table 1). The distance distribution function $P(r)$ calculated from the SAXS data indicates a maximum diameter $D_{\max} \sim 137$ Å (Fig. 7d). We calculated an electron density from solution scattering data using DENSS (Supplementary Table 3), which is shaped like a ‘fidget spinner’ with two smaller ‘feet’ domains and a slightly larger ‘hood’ domain sitting on top. We interpreted this density by docking the crystal structures the p65 and p50 DNA-binding domains solved in the presence of DNA³⁷ inside the feet domains, which are loose with respect to the dimerization domain in the absence of DNA. In contrast, the crystal structure of Δ IBB-importin $\alpha 3$ bound to p65/p50-NLSs was manually docked into the larger hood density, which is perched perpendicular to the p50/p65 heterodimer (Fig. 8a). The directionality of importin $\alpha 3$ with respect to the p50/p65 core was determined based on the NLS-peptide bound to the major (p50) and minor (p65) NLS-binding sites that accurately position the N- and C-termini of importin $\alpha 3$ close to p50 and p65, respectively. This pseudo-atomic model was refined against the DENSS density using rigid-body refinement, yielding an excellent agreement between the atomic model and SAXS-data ($\chi^2 = 1.50$) (Supplementary Fig. 7a).

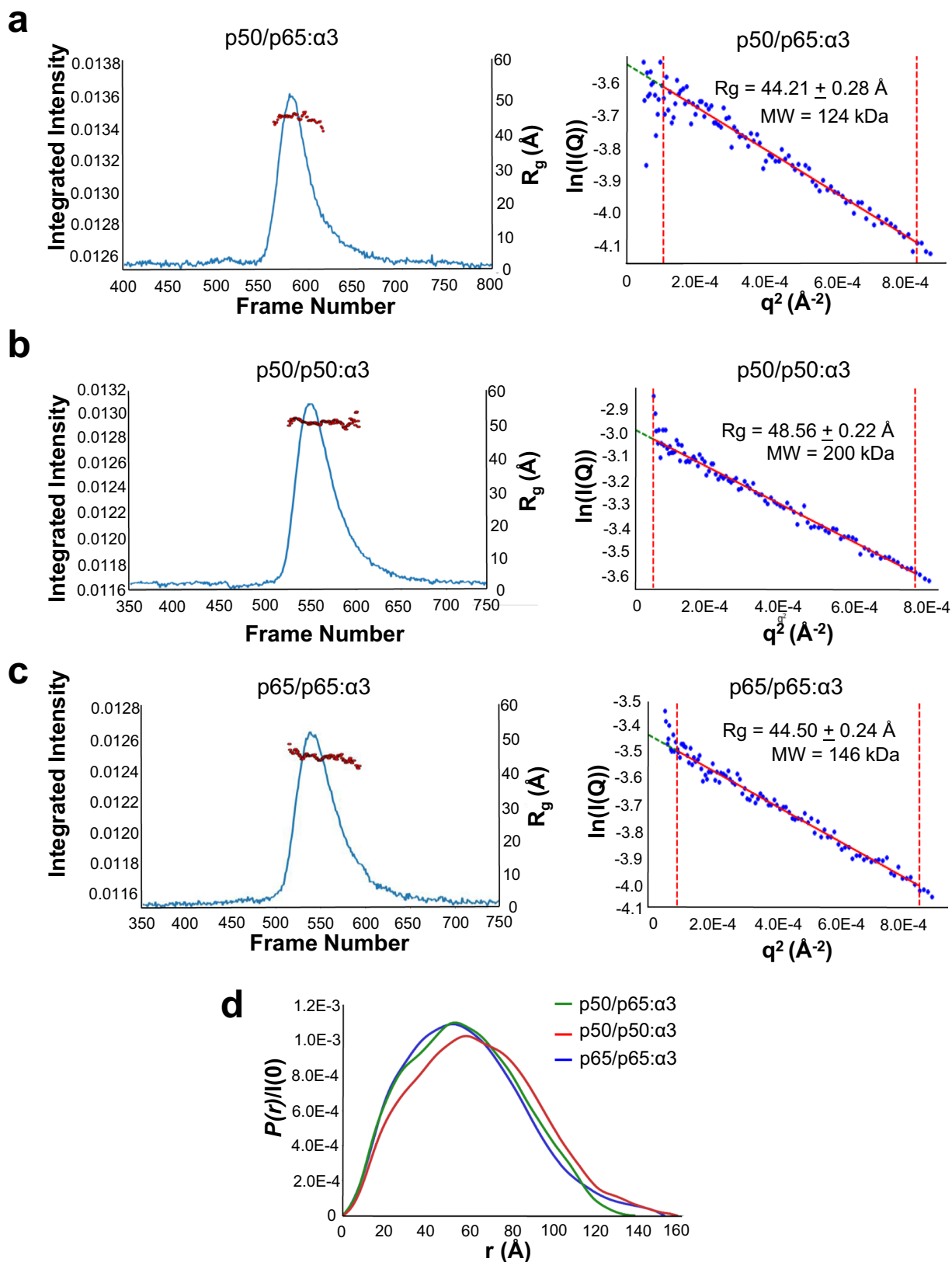
We also studied the solution structure of homodimeric p50/p50 and p65/p65 bound to Δ IBB-importin $\alpha 3$ (Supplementary Table 3). The p50/p50: Δ IBB-importin $\alpha 3$ complex appeared larger in solution than the p50/p65: Δ IBB-importin $\alpha 3$ complex, with an R_g of 48.56 ± 0.22 Å (Fig. 7b) corresponding to an approximate hydrated mass of 200 ± 20 kDa. This observation is consistent with a bi-dimeric complex containing two importins $\alpha 3$ per p50/p50 homodimer (stoichiometry 2:2) with MW ~ 185.2 kDa (Supplementary Table 1). The distance distribution function $P(r)$ calculated from the SAXS data indicates a maximum diameter $D_{\max} \sim 157$ Å (Fig. 7d). The calculated electron density from DENSS has four lobes with two ‘feet’ and two ‘arms’ protruding upward. We interpreted the density by docking in the p50 DNA-binding domain solved without the DNA in the feet domain, the dimerization domain projecting into the center, and two crystal structures of the Δ IBB-importin $\alpha 3$ bound to p50-NLSs manually docked into the density (Fig. 8b). The pseudo-atomic model was refined against the DENSS density using rigid-body refinement, yielding an excellent agreement between the atomic model and SAXS-data ($\chi^2 = 1.29$) (Supplementary Fig. 7b). In contrast, the p65/p65: Δ IBB-importin $\alpha 3$

complex has an R_g of 44.50 ± 0.24 Å (Fig. 7c, Supplementary Table 3), corresponding to an approximate hydrated mass of 146 ± 14.6 kDa, close to a 1:1:1 complex (MW ~ 125.4 kDa) (Supplementary Table 1), as observed for the p50/p65 heterodimer. The distance distribution function $P(r)$ calculated from the SAXS data indicates a maximum diameter $D_{\max} \sim 151$ Å, which is slightly larger than the p50/p65: Δ IBB-importin $\alpha 3$ complex (Fig. 7d). The calculated electron density from DENSS is also shaped like a fidget spinner with the importin $\alpha 3$ perched laterally instead of perpendicular to the dimerization domain (Fig. 8c), similar to the p50/p65: Δ IBB-importin $\alpha 3$. We interpreted the density by docking the p65 DNA-binding domain solved without the DNA (PDB: 1RAM) in the feet domain, the dimerization domain projecting into the center, and manually docked the crystal structures of the Δ IBB-importin $\alpha 1$ bound to p65-NLSs into the density. The pseudo-atomic model was refined against the DENSS density using rigid-body refinement, yielding an excellent agreement between the atomic model and SAXS-data ($\chi^2 = 1.71$) (Supplementary Fig. 7c). Interestingly, these results suggest both NF- κ B complexes containing the p65-NLS binds one equivalent of importin $\alpha 3$, consistent with a 1:1:1 quaternary structure. Meanwhile, in the p50/p50 homodimer, the p50-NLS binds two copies of importin $\alpha 3$, consistent with a 2:2 quaternary structure. Thus, the NF- κ B complex composition is the key determinant for asymmetric recognition by importin $\alpha 3$.

Discussion

The specificity of importin $\alpha 3$ for the canonical NF- κ B p50/p65 heterodimer was first reported over fifteen years ago^{19,20}. However, the mechanisms of NF- κ B nuclear import have remained poorly studied, despite the vital role of this transcription factor in cell physiology and disease. In this paper, we elucidate the structural basis governing the recognition of canonical NF- κ B heterodimer and homodimers by the isoform importin $\alpha 3$.

NF- κ B p50/p65 subunits generate a bipartite NLS in trans. We provide biochemical (Fig. 2) and biophysical (Fig. 7) evidence that the p50, p65, and importin $\alpha 3$ assemble into a 1:1:1 heterotrimeric complex, supporting a previous model¹⁹. The p50- and p65-NLSs are recognized asymmetrically by importin $\alpha 3$, which sequesters them at the major and minor NLS-pocket, respectively. This recognition is similar to that described for the dimeric transcription factor STAT1, which is also recognized asymmetrically by importin $\alpha 5$ ^{26,27}. However, NF- κ B is more complex than STAT1 due to the existence of different dimeric complexes in living cells. We found that all p65-containing NF- κ B dimers assembled into a 1:1:1 complex with importin $\alpha 3$, while the p50/p50 homodimer assembled in a 2:2 complex. These results suggest the p65 subunit is key to introduce asymmetry in the NF- κ B nuclear import complex. Crystallographic and SAXS studies revealed that the two NF- κ B subunits generate a bipartite NLS in trans, similar to some oligomeric viral complexes^{25,62} that expose multiple NLSs on their quaternary structure^{25,79}. While the NF- κ B p50/p65 resembles a bipartite NLS-like cargo, it does not show the classical bipartite NLS interdependence where both NLS boxes are necessary, and mutation of either cluster of basic residues significantly impacts importin α binding, at least in vitro⁶³. In our binding studies (Fig. 3a), only the p50-NLS was indispensable for importin $\alpha 3$ association, suggesting this NLS is the primary determinant for nuclear import, in agreement with a prior transfection study¹⁹. Our crystal structures help rationalize this specificity by showing that p50- and p65-NLSs bind more intimately to importin $\alpha 3$ than importin $\alpha 1$. The p50-NLS occupies the major NLS pocket making 18 hydrogen bonds and



two salt bridges in complex with importin α3 versus only nine hydrogen bonds with importin α1.

Similarly, the binding of the p65-NLS to importin α3 is also energetically more favorable than importin α1. Unexpectedly, the p65-NLS adopts two strikingly different conformations bound to importin α3 or α1. It is fully extended and stretched with

importin α1, both at the major and minor NLS pockets (Fig. 6f, h), while it binds to the importin α3 minor NLS pocket in an extended conformation up to the P₃' position but is helical from the P₄' position onward (Fig. 6d). A helical conformation of the NLS backbone has been previously reported^{15,17,64}, though it remains relatively rare, as most NLSs

Fig. 7 SEC-SAXS analysis of pre-formed NF- κ B/ Δ IBB-importin α 3 complexes. **a** SEC-SAXS profile of a preassembled p50/p65/ Δ IBB-importin α 3 complex at 4.5 mg ml⁻¹ measured in 20 mM Tris-HCl pH 7.0, 0.175 M NaCl, 2.5% glycerol and 0.5 mM TCEP at 4 °C. The red dots indicate R_g values (on the Y-axis) corresponding to frames on the X-axis. The right panel shows the Guinier plot calculated from averaging buffer-subtracted scattering intensities from frames (465–484) and the sample peak (571–599) (red dots). The p50/p65/ Δ IBB-importin α 3 coefficient of determination for a best-fit line, R^2 , is 0.9564 (red line). **b** SEC-SAXS profile of the pre-formed p50/p50/ Δ IBB-importin α 3 complex at 6.29 mg ml⁻¹ measured in 20 mM Tris-HCl pH 7.5, 0.15 M NaCl, 2.5% glycerol and 0.5 mM TCEP at 4 °C. The red dots indicate R_g values (on the Y-axis) corresponding to frames on the X-axis. On the right side is a Guinier plot calculated from averaging buffer-subtracted scattering intensities from frames (180–242) and the sample peak (547–556) (red dots). The p50/p50/ Δ IBB-importin α 3 coefficient of determination for a line of best fit, R^2 , is 0.9766 (red line). **c** SEC-SAXS profile of the pre-formed p65/p65/ Δ IBB-importin α 3 complex at 6.60 mg ml⁻¹ measured in 20 mM Tris-HCl pH 7.5, 0.15 M NaCl, 2.5% glycerol and 0.5 mM TCEP at 4 °C. The red dots indicate R_g values (on the Y-axis) corresponding to frames on the X-axis. The Guinier plot (right panel) was calculated from averaging buffer-subtracted scattering intensities from frames (72–118) and the sample peak (538–550) (red dots). The p65/p65/ Δ IBB-importin α 3 coefficient of determination for the line of best fit, R^2 , is 0.9712 (red line). **d** $P(r)$ function plots calculated from SEC-SAXS data for p50/p65/ Δ IBB-importin α 3 (green), p65/p65/ Δ IBB-importin α 3 (blue) and p50/p50/ Δ IBB-importin α 3 (red) complexes.

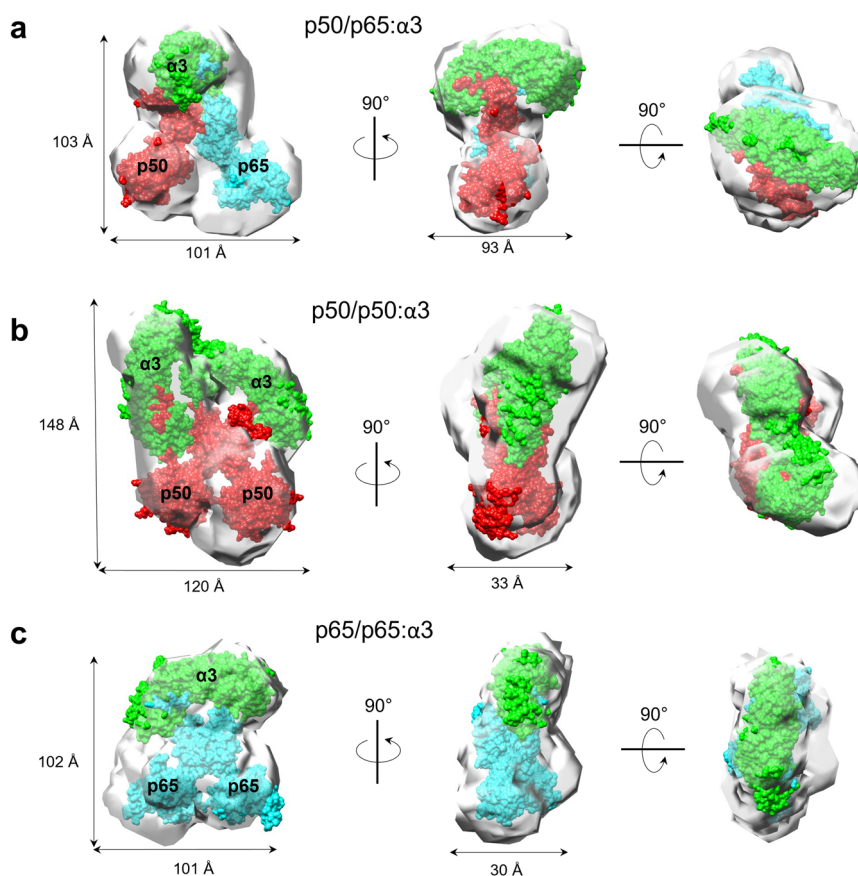


Fig. 8 Solution structures of the NF- κ B import complexes. Ab initio SEC-SAXS electron density of **a** p50/p65/ Δ IBB-importin α 3, **b** p50/p50/ Δ IBB-importin α 3 (**c**) and p65/p65/ Δ IBB-importin α 3. All DENSS densities are shown as semitransparent surfaces. The crystallographic structures of Δ IBB-importin α 3 (green), p50/p50 (PDB: 1NFK) (red) and p65/p65 homodimers (PDB: 1RAM) (blue), and p50/p65 heterodimer (blue/red) (PDB: 1VKX) were docked inside the density and are shown as a surface representation. The agreement between solution and modeled crystal structures was calculated using the FoXS server and shown in Supplementary Fig. 7.

bind importin α in an extended conformation to maximize binding contacts with the NLS-binding pocket. Similar to other helical NLSs^{15,17,64}, the C-terminal region of the p65-NLS contains aromatic residues, like Tyr306 and Phe309. NMR studies found the region of p65 encompassing the NLS to be predominantly random coil in solution, but it folds into helix 3 (res. 293–304) and helix 4 (res. 306–315) in complex with I κ B^{41,42,65–67}. While our data suggests the p65-NLS is not a major binding determinant for importin α 3 in the p50/p65 heterodimer, it is a functional NLS for the p65/p65 homodimer (Fig. 3b). In the absence of p50, the p65-NLS binds the major NLS site, mimicking the p50-NLS (Fig. 5e). If the p65-NLS is not a major determinant

for nuclear import of p50/p65, why is it intimately bound at the minor NLS-site of importin α 3? The answer to this question may be unrelated to nuclear import. Prior research found Set9-mediated methylation of p65 Lys314 and Lys315 results in degradation of the activated NF- κ B complex and down-regulation of NF- κ B gene expression⁶⁸. The p65 residues Lys314 and Lys315 are inaccessible in complex with importin α 3, possibly preventing Set9-mediated methylation. Thus, the p65-NLS binding at the minor NLS pocket may reflect a regulatory mechanism to sequester a critical region of p65 from cellular binding partners, preventing post-translational modifications from inactivating NF- κ B signaling.

Importin $\alpha 3$ flexibility mediates NF- κ B specificity. Structural comparison between the p50- and p65-NLSs bound conformations of importin $\alpha 1$ and $\alpha 3$ revealed a hinge region in Arm 4 and a region of shear motion of Arm 7 of importin $\alpha 3$, which results in conformational changes within the major and minor NLS-pocket absent in the more rigid importin $\alpha 1$ (Fig. 5c, g). This observation is in line with recent work on other NLS-cargos recognized preferentially by importin $\alpha 3$, such as SOX2 and the Henipavirus W proteins that concluded specificity for importin $\alpha 3$ requires repositioning of Arm 7, which is more rigid in importin $\alpha 1$ ^{24,58}. Another study found RCC1 specificity for importin $\alpha 3$ is due to the drastic conformational changes between Arms 1 and 4 required to accommodate a bulky β -propeller domain adjacent to the NLS²¹. Molecular dynamics simulations⁷ also provided evidence that importin $\alpha 3$ is a flexible solenoid that undergoes segmented motion in response to cargo-binding. Precisely, the N- and C-terminal arms move as rigid bodies with respect to the central core, allowing this isoform to open and close to accommodate bulky domains flanking an NLS, as seen for RCC1²¹ and SOX⁵⁸ or extend in response to elongated bipartite NLSs, as seen for Henipavirus W protein²⁴ and Influenza Pb2⁷. The common denominator of all importin $\alpha 3$ cargos is a complex structural topology, whereby the NLS is exposed onto the tertiary or quaternary structure of an oligomeric structure, as seen for the NF- κ B p50/p65 heterodimer. Importin $\alpha 3$ conformational flexibility allows this isoform to associate with topologically complex cargos by undergoing local conformational changes that maximize NLS association. We proposed that this molecular recognition is equivalent to an induced fit for NLS-cargos.

Mutually exclusive binding of I κ B α and importin $\alpha 3$ to NF- κ B p50/p65. Two crystal structures of p50/p65 bound to I κ B α revealed the inhibitor binds specifically to the p65-NLS^{41,69}, while the p50-NLS is solvent-exposed and potentially available for importin $\alpha 3$ binding in the inhibited state. In parallel, shown in this paper, the p50-NLS is the predominant determinant for p50/p65 binding (Fig. 3a). Our competition studies using purified I κ B α , importin $\alpha 3$, and pre-formed complexes of the two proteins with p50/p65 (Fig. 4) revealed that not only is importin $\alpha 3$ unable to dissociate I κ B α from p50/p65, but the import adapter also fails to associate with a pre-formed p50/p65:I κ B α complex. Thus importin $\alpha 3$ is unlikely to shuttle the NF- κ B:I κ B α complex through the NPC⁷⁰, as suggested by treating unstimulated cells with the Crm1-inhibitor leptomycin B^{71–73}. As previously pointed out⁷⁴, shuttling of the inhibited p50/p65:I κ B α complex was only observed in the presence of leptomycin B, whereas all biochemical approaches failed to detect nuclear NF- κ B:I κ B complexes in unstimulated cells⁷⁴, arguing that the shuttling of the inhibited p50/p65 complex could reflect an artificial result associated with the use of leptomycin B.

Furthermore, since I κ B α does not bind directly to the p50-NLS, which we found is the predominant NLS in p50/p65, the inhibitor must prevent importin $\alpha 3$ binding to the p50-NLS through steric hindrance, rather than direct competition for the same moiety. Overall, these data challenge the classical paradigm of NF- κ B retention⁷⁵, which explains p50/p65 cytoplasmic retention as a direct consequence of masking the p65-NLS. Instead, I κ B α appears to be a non-competitive inhibitor of the p50-NLS that prevents importin $\alpha 3$ binding to the p50/p65:I κ B α complex by a structural mechanism possibly involving steric hindrance rather than direct competition for the NF- κ B NLSs. Thus, NF- κ B p50/p65 nuclear import is only possible after I κ B α has been degraded (Fig. 9a).

The implication of NF- κ B nuclear transport for transcription.

NF- κ B nuclear localization is a highly regulated import pathway, and its dysregulation is linked to several human diseases, including cancer³¹. Upon nuclear localization, the NF- κ B dimers exhibit distinctly different transcriptional properties: the p50/p65 and p65/p65 complexes promote gene expression via their C-terminal transactivation domain, whereas the p50/p50, lacking a transactivation domain, suppresses gene expression. Both p65/p65 and p50/p50 homodimers are less abundant than p50/p65 in vivo and possess biological activities (activation and repression, respectively) independently regulated to ensure sustained gene expression⁷⁶. The p65/p65 is the least stable NF- κ B dimer, and while its concentration is likely low, this homodimer can also be inhibited and retained in the cytoplasm by I κ B α ⁴⁴ (Fig. 9b). However, less clear is why the p50/p50 homodimer is excluded from the nucleus. This dimeric transcription factor contains two potent NLSs and functions as a transcription ‘repressor’ due to its ability to occupy κ B sites and suppress gene expression^{77–79}. The data presented in this paper lead us to hypothesize that human cells evolved several different cellular mechanisms to favor p50/p65 nuclear translocation over the p50/p50 complex. First, the relative concentration of p50/p50 homodimer is low compared to the more abundant p50/p65 heterodimer due to the reduced stability of the p50/p50 dimerization interface compared to the p50/p65 heterodimer^{37,38,41,42}. Second, as demonstrated in this paper, the p50-NLS binds exclusively the major NLS-binding site of importin α , which results in a large, bi-dimeric import complex p50/p50/(α/β)₂ (Fig. 9c), that is energetically more costly to translocate into the nucleus than smaller cargos^{80,81} such as p50/p65 and p65/p65. As a result, nuclear import for cargos requiring multiple copies of importin α/β like the p50/p50 complex is likely disfavored and out-competed by cargos that require only a single importin α/β like p50/p65. Finally, NF- κ B complexes maturation and NLS exposure utilize different signaling cascades, which impart energetic differences between the p50/p65 and p65/p65 complexes compared to the p105/p50 precursor complex. In the NF- κ B canonical signaling pathway, the p50/p65 and p65/p65 maturation are less energetically costly than the p105/p50 maturation, which requires IKK-mediated phosphorylation, ubiquitination, and ATP-dependent proteasomal degradation of the p105 ARD domain⁵². These energetic and kinetic barriers suggest the nuclear translocation of the p50/p50 homodimer is less efficient than the p50/p65 heterodimer, ensuring appropriate gene expression and healthy cellular signaling.

In conclusion, this paper describes the mechanisms of NF- κ B dimer recognition by the isoforms $\alpha 3$. Our work paves the way to identifying inhibitors that target the p50-NLS:importin $\alpha 3$ association, reducing the accumulation of NF- κ B in the nucleus and dampening aberrant NF- κ B signaling.

Methods

DNA, plasmids, and peptides. The plasmids encoding human p65 (residues 1–306) and Δ NLS-p50 (residues 41–351) cloned in the pLM1 vector were a generous gift of Dr. Stephen Harrison⁴¹. Δ NLS-p65 (residues 1–290) was generated by introducing a stop codon at position D291 of p65 using the QuikChange site-directed mutagenesis kit (Stratagene). A synthetic gene encoding human p50 (residues 1–366), p50 lacking the DNA-binding domain Δ DBD-p50, residues 243–366), and p65 lacking the DNA-binding domain Δ DBD-p65, residues 191–316) were purchased from Genewiz and cloned between BamHI and XhoI restriction sites of expression vectors pGEX-6P-1 (GE Life Sciences). Plasmids encoding Δ IBB-importin $\alpha 1$ (residues 70–529) and Δ IBB-importin $\alpha 3$ (residues 68–487 and 63–487) were cloned into vectors pET-30a and pGEX-6P or pET-15b, respectively, as previously described^{7,21}. Untagged I κ B α (residues 67–287) was cloned in the pET-11a^{65–67}. Peptides encompassing the p65-NLS (294-DRHRIEKRKRITRYETFKSIMKK-315) and p50-NLS (355-DKEEVQRKRQKLMF-368) were synthesized from GenScript (Piscataway, NJ).

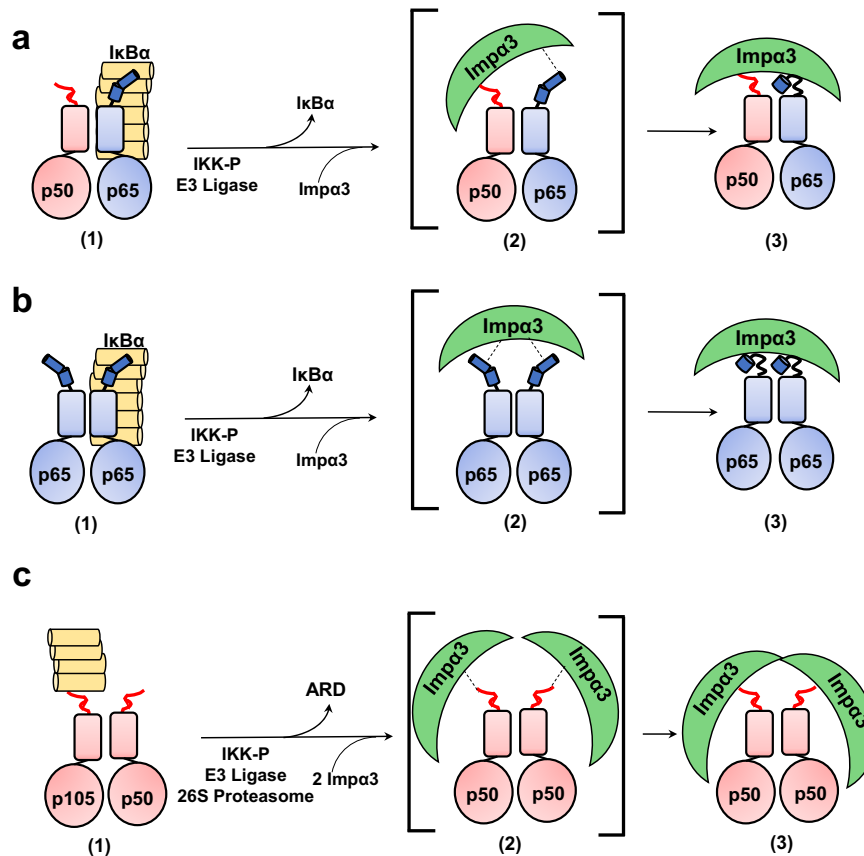


Fig. 9 Recognition of NF- κ B dimers by importin α 3. **a** Schematic diagram of the steps leading to exposure of NLS, binding, and nuclear import of the NF- κ B complexes of **a** p50/p65, **b** p65/p65, and **c** p50/p50. On the left is the cytoplasmic conformation inhibited by I κ B α through masking of the p65-NLS for p50/p65 and p65/p65 complexes or by the ARD domain masking the p50-NLS in p105/p50 complex (1). Upon activation by stimuli, the inhibited complexes are liberated by either dissociation of I κ B α in p50/p65 or p65/p65 complexes or cleavage of the ARD domain in the p50/p50 complex by IKK, E3 Ligase, and 20S proteasome, which expose two NLSs for recognition by importin α 3 (2). On the right is the competent import conformation recognized by importin α 3 that binds the exposed NLS on the surface of the NF- κ B complexes (3).

Recombinant protein expression and purification. Expression plasmids for all human p65, p50 (and relative mutants), Δ I κ B-Importin α 1, Δ I κ B-Importin α 3 were transformed and expressed in BL21 DE3 *E. coli* strain in the presence of ampicillin or kanamycin. Plasmids encoding GST- Δ DBD-NF- κ B and Δ I κ B-Importin α 3 were co-transformed in BL21 DE3 *E. coli* strain and expressed in the presence of ampicillin and kanamycin. Bacterial cultures were grown in LB medium at 37 °C until $A_{600} = \sim 0.6$ AU and all p65 induced at 16 °C with 0.25 mM IPTG for 12–16 h, all p50 induced at 18 °C at 0.25 mM IPTG for 12–16 h, and all importin α 1 and α 3 at 28 °C with 0.5 mM IPTG for 4 h. Cell pellets expressing all untagged p65 and p50 constructs (with or without the C-terminal NLS) were sonicated in lysis buffer 1 (20 mM HEPES, pH 7.5, 400 mM NaCl, 2 mM EDTA, 2 mM DTT, 1 mM PMSF, 5% (v/v) glycerol) followed by 0.2% polyethyleneimine precipitation for 1 h at 4 °C and 55% ammonium sulfate precipitation for 2 h at 4 °C. The p65, Δ NLS-p65, and Δ NLS-p50 ammonium sulfate pellets were re-suspended in Re-Suspension Buffer (20 mM HEPES, pH 7.5, 2 mM DTT, 2 mM EDTA, 0.2 mM PMSF, 5% (v/v) glycerol), loaded onto 5 mL HiTrapTM SP HP Column (GE Healthcare), washed with 5 CV of Buffer A (20 mM Tris, pH 7.5, 50 mM NaCl, 5 mM β -Mercaptoethanol, 2 mM EDTA, 0.2 mM PMSF), and the proteins were eluted using a linear gradient from 0% to 100% Buffer B (20 mM Tris, pH 7.5, 500 mM NaCl, 5 mM β -Mercaptoethanol, 2 mM EDTA, 0.2 mM PMSF). Cell pellets expressing GST-p50, GST- Δ DBD-p50, GST- Δ DBD-p65 and co-expressed GST- Δ DBD-NF- κ B and Δ I κ B-Importin α 3 complexes were sonicated in Lysis Buffer 2 (20 mM Tris, pH 8.0, 250 mM NaCl, 1 mM PMSF, 5 mM BME, 0.1% (v/v) TWEEN 20, 1 mM EDTA), followed by 0.2% polyethyleneimine precipitation for 1 hour at 4 °C. GST-p50, GST- Δ DBD-p50, GST- Δ DBD-p65, and GST- Δ DBD-NF- κ B: Δ I κ B-Importin α 3 complexes were purified by affinity chromatography on Glutathione Resin (GenScript) and incubated overnight with 100 U of PreScission Protease in PPase Cleavage Buffer (20 mM Tris-HCl, pH 7.0, 150 mM NaCl, 1 mM DTT, 1 mM EDTA, 0.1% (v/v) TWEEN 20). Untagged p50, Δ DBD-p50, Δ DBD-p65, and Δ DBD-NF- κ B: Δ I κ B-Importin α 3 complexes were recovered off the beads. All GST-tagged⁷ and His-tagged Δ I κ B-Importin α 1 and α 3²¹ were purified as previously described. I κ B α was expressed and purified as previously described^{65–67}. All purified samples were concentrated with a 10- or 30 kDa Millipore PES concentrator and injected on a Superdex 200 16/60 column (GE Healthcare) pre-

equilibrated with Gel Filtration Buffer 1 (20 mM Tris-HCl pH 7.5, 150 mM NaCl, 5 mM β -Mercaptoethanol, 2% (v/v) glycerol). Sample purity was confirmed by SDS-PAGE (13.5%) analysis. Complexes eluted from beads were further purified on a Superdex 200 16/60 column (GE Healthcare) pre-equilibrated with Gel Filtration Buffer 1. Co-purified Δ DBD-NF- κ B: Δ I κ B-Importin α 3 complexes were further purified on a Superdex75 10/300 column (GE Healthcare).

Complex assembly. Heterodimeric p50/p65 complexes (e.g., p50/p65, p50/ Δ NLS-p65, Δ NLS-p50/ Δ NLS-p65) were assembled by incubating in a 1:1.5 p50:p65 molar ratio, respectively, together at 25 °C for 30 min, then at 37 °C for 1 h, followed by centrifugation at 12,000 \times g at 4 °C for 30 min to remove precipitation⁴¹. Homodimeric NF- κ B (p65/p65, p50/p50, Δ NLS-p65/ Δ NLS-p65, Δ NLS-p50/ Δ NLS-p50, Δ DBD-p65/ Δ DBD-p65, Δ DBD-p50/ Δ DBD-p50) complexes were concentrated with a 30 kDa Millipore PES concentrator and injected on a Superdex 200 16/60 column (GE Healthcare) pre-equilibrated with GF Buffer 1. All NF- κ B trimeric complexes were assembled by incubating pre-formed NF- κ B hetero/homodimers in a 1.5-molar excess of Δ I κ B-Importin α 3 or I κ B α , followed by incubation at 4 °C for 1 h. Complexes were concentrated with a 30 kDa Millipore PES concentrator and injected on a Superose 12 10/30 GL column (GE Healthcare) pre-equilibrated with GF Buffer 1 followed by SDS-PAGE analysis. Trimeric complexes of NF- κ B p50 or p65 dimerization domains bound to importin α 3 Δ DBD-p50/ Δ DBD-p50: α 3 and Δ DBD-p65/ Δ DBD-p65: α 3, Supplementary Fig. 2) were formed by co-expression in bacteria. Supplementary Table 1 reports the expected MWs for all the complexes assembled in this study.

ELISA-based microtiter binding assay, native gel electrophoresis. For microtiter binding assay⁴, NF- κ B hetero/homodimers (200 ng in 100 μ L 0.05 M carbonate bicarbonate buffer, pH 9.6) were coated on ELISA plates (Nunc MaxiSorp Flat-Bottom Plate, 44-2404-21) and incubated at 4 °C overnight. The plates were blocked with PBS containing 5% skim milk for 2 h at room temperature and were washed three times with PBS containing 0.05% Tween-20 (PBST). The His-Importin α samples were diluted in PBST (from 1000 to 0 nM) and 100 μ L added into the wells, and the plates were incubated at room temperature for 1 h. The

plates were washed three times with PBST and incubated with anti-6xHis-4HRP-conjugated rabbit polyclonal antibody (1:3500) (Abcam ab1187) for 1 h at 37 °C. After washing with PBST three times, the reaction was initiated by the addition of 100 μ L of tetramethylbenzidine (TMB) substrate (1-Step Ultra TMB-ELISA (Ref 34028), Thermo Scientific). The colorimetric reaction was stopped by adding 100 μ L of 2 M H₂SO₄, and absorbance was read at 450 nm wavelength using a Tecan microplate reader. All experiments were carried out in duplicates. One-site specific binding analysis using least-squares fit was performed using GraphPad Prism 9 for Windows, GraphPad Software, LLC (version 9.2.0). Native gel electrophoresis was performed on a 1.5% agarose gel, as previously described⁸². In the p50/p65:α titration assay in Fig. 2, 10 μ g of ΔIBB-importin α1 and ΔIBB-importin α3 were incubated with increasing concentrations of the pre-assembled p50/p65 heterodimers. For the competition assay in Fig. 4, 10 μ g of p50/p65 heterodimer was incubated for one hour at 4 °C with increasing molar equivalents of ΔIBB-importin α3 or IκBα. Similarly, pre-formed trimeric p50/p65:α3 or p50/p65:IκBα complexes were challenged with increasing concentrations of either ΔIBB-importin α3 or IκBα. The mixture was separated on a 1.5% agarose gel at 4 °C for 2 h at 50 V. After electrophoresis the gel was fixed in Gel Fixing solution (25% (v/v) isopropanol and 10% (v/v) acetic acid) for 20 min and then equilibrated with 95% (v/v) ethanol for 2 h. Gels were then dried, stained for 10 min in 0.4% (w/v) Coomassie brilliant blue R250 in Gel Fixing solvent, and destained in Gel Fixing solvent until the background was clear.

Crystallographic methods. His-ΔIBB-importin α1 and α3 were concentrated to ~15–20 mg ml⁻¹ and crystallized using the vapor diffusion hanging drop method by mixing 2 μ l of purified protein with 0.5 μ l containing a 2.5-fold molar excess of NLS peptide. The best crystals for ΔIBB-importin α3 bound to p50-NLS were obtained using 0.2 M potassium thiocyanate, 20% PEG3350, 0.1 M BIS-TRIS pH 6.5. ΔIBB-importin α3 bound to both the p50- and p65-NLS peptides was crystallized in the presence of 0.2 M ammonium sulfate, 0.1 M BIS-TRIS pH 6.5, 25% PEG 3350. For ΔIBB-importin α1, all complexes with the p50-NLS and p65-NLS alone or p50-NLS + p65-NLS peptides were crystallized in the presence of 0.5–0.65 M sodium citrate, 0.1 M HEPES pH 6.0, 10 mM β-Mercaptoethanol. All crystals were harvested in nylon cryo-loops, cryo-protected with 27% ethylene glycol, and flash-frozen in liquid nitrogen. Complete diffraction data were collected at beamlines 9-2 and 12-1 at the Stanford Synchrotron Radiation Lightsource (SSRL) on a Dectris Pilatus 6 M detector (Table 1). The structure of ΔIBB-importin α3 bound to the p50-NLS was solved by molecular replacement (MR) using the open ΔIBB-importin α3 (PDB: 6BVV) as a search model, as implemented in PHASER⁸³ (version 2.8). The p50-NLS was built in an unbiased Fo-Fc electron density map using Coot⁸⁴ (version 0.9.4), and the model was subjected to several rounds of real-space refinement using *phenix.real_space_refine*⁸⁵ (version 1.18.2-3874) in combination with reciprocal-space and TLS refinement using *phenix.refine*⁸⁶ (version 1.18.2-3874). This model was then used as a search template to solve the structure of ΔIBB-importin α3 bound to both the p65- and p50-NLSs, also using PHASER⁸³. The p65-NLS and p50-NLS were modeled in unbiased Fo-Fc densities readily visible at the minor and major NLS-binding pockets, respectively, using Coot⁸⁴. The complete model of ΔIBB-importin α3/p50-NLS/p65-NLS was refined as described above. The final models of ΔIBB-importin α3 bound to just the p50-NLS or both the p65- and p50-NLSs have a $R_{\text{work}}/R_{\text{free}}$ of 19.9/22.0 and 19.6/23.7, at 2.10 and 2.85 Å resolution, respectively (Table 1). For ΔIBB-importin α1, both complexes with the p50-NLS and p50/p65-NLSs were solved by molecular replacement (MR) using the rigid structure of ΔIBB-importin α1 (PDB: 3Q5U) as a search model, as implemented in PHASER⁸³. Atomic models for the NF-κB NLSs were built using Coot⁸⁴ and refined using *phenix.refine*⁸⁶. The final models of ΔIBB-importin α1 bound to p50-NLS, p65-NLSs, or both p65/p50 peptides were refined to an $R_{\text{work}}/R_{\text{free}}$ of 20.0/23.5, 19.1/21.8, and 19.8/24.1, at 2.82, 2.24, and 2.40 Å resolution, respectively. Final stereochemistry was validated using MolProbity⁸⁷. Data collection and refinement statistics are summarized in Table 1.

Size exclusion chromatography coupled to small angle X-ray scattering.

SEC-SAXS analysis was performed at ID7A1 station at MacCHESS, which is equipped with an AKTA Pure FPLC system (GE Healthcare). The trimeric p50/p65:ΔIBB-importin α3, p65/p65:ΔIBB-importin α3 and p50/p50:ΔIBB-importin α3 complexes were pre-assembled and concentrated at 4.5, 6.6, and 6.29 mg ml⁻¹, respectively. At the beamline, pre-formed complexes were injected on a Superdex 200 10/300 GL column (GE Healthcare) equilibrated in SEC-SAXS Buffer (20 mM Tris-HCl pH 7.0, 175 mM NaCl, 2% glycerol, and 0.5 mM TCEP). SAXS data were recorded on an EIGER 4 M detector (Dectris Ltd. Baden, Switzerland) in vacuo at 2 s per frame with a fixed camera length of 1.709 m and 10.03 keV (1.237 Å) energy allowing the collection of the angular range q between 0.008 and 0.54 Å⁻¹. Primary reduction of the SAXS data was performed using RAW⁸⁸ (versions 1.6.4 and 2.0.3), and ATSAS software⁸⁹ (version 2.6.0). To minimize the effects of damaged material accumulating on the X-ray sample window and to help compensate for any baseline drift, the buffer profile was constructed by averaging the frames before the sample peak frames. The Guinier plots of the subtracted profiles were linear to the lowest measured q value. GNOM⁹⁰ was used to calculate $P(r)$ plots from the scattering data. Ab initio model calculations to generate an average electron density

from solution scattering data were done using DENSS⁹¹, as implemented in RAW. The DENSS densities have a Fourier shell correlation (FSC) of 52.2 Å (p50/p65/ΔIBB-importin α3), 64.7 Å (p50/p50/ΔIBB-importin α3) and 50.7 Å (p65/p65/ΔIBB-importin α3), respectively. Docking of PDB models inside the SAXS density was done manually and improved by rigid-body refinement using Chimera⁹². Theoretical solution scattering curves were calculated using the FoXS web server⁹³. SEC-SAXS data collection and analysis statistics are in Supplementary Table 3.

Structure analysis and modeling. All structural illustrations were generated using PyMol (Schrödinger, Inc.) and Chimera⁹². Binding interfaces were analyzed using PISA⁵⁵ and PDBsum⁹⁴. Secondary structure superimpositions were done in Coot⁸² and analyzed using SuperPose 1.0 server⁵⁹. DynDom⁵⁶ was used to identify importin α3 domain movements upon cargo-binding.

Reporting summary. Further information on research design is available in the Nature Research Reporting Summary linked to this article.

Data availability

Coordinates and structure factors for the ΔIBB-importin α3 + p50-NLS, ΔIBB-importin α3 + p50-NLS + p65-NLS and ΔIBB-importin α1 + p65-NLS, ΔIBB-importin α1 + p50-NLS, and ΔIBB-importin α1 + p50-NLS + p65-NLS complexes have been deposited in the Protein Data Bank (accession codes 7LFC, 7LFA, and 7LEU, 7LEQ, 7LET). Additionally, all other PDBs analyzed in this study include 1NFK, 1RAM, 1VKX, 6BVV, 3Q5U, 6BVZ, 6WX8, and 5TBK. SEC-SAXS and all other data are available from the corresponding author upon reasonable request. Source data are provided with this paper.

Received: 21 May 2021; Accepted: 11 February 2022;

Published online: 08 March 2022

References

1. Bednenko, J., Cingolani, G. & Gerace, L. Importin beta contains a COOH-terminal nucleoporin binding region important for nuclear transport. *J. Cell Biol.* **162**, 391–401 (2003).
2. Macara, I. G. Transport into and out of the nucleus. *Microbiol. Mol. Biol. Rev.* **65**, 570–594 (2001).
3. Stewart, M. Molecular mechanism of the nuclear protein import cycle. *Nat. Rev. Mol. Cell Biol.* **8**, 195–208 (2007).
4. Mackmull, M. T. et al. Landscape of nuclear transport receptor cargo specificity. *Mol. Syst. Biol.* **13**, 962 (2017).
5. Aramburu, I. V. & Lemke, E. A. Floppy but not sloppy: interaction mechanism of FG-nucleoporins and nuclear transport receptors. *Semin. Cell Dev. Biol.* **68**, 34–41 (2017).
6. Cingolani, G. & Gerace, L. Molecular basis of nucleocytoplasmic transport. In *Handbook of Cell Signaling* (eds Bradshaw, R. & Dennis, E.) Vol. 3 419–429 (Academic Press, 2002).
7. Pumroy, R. A., Ke, S., Hart, D. J., Zachariae, U. & Cingolani, G. Molecular determinants for nuclear import of influenza A PB2 by importin alpha isoforms 3 and 7. *Structure* **23**, 374–384 (2015).
8. Lott, K. & Cingolani, G. The importin beta binding domain as a master regulator of nucleocytoplasmic transport. *Biochim. Biophys. Acta* **1813**, 1578–1592 (2011).
9. Weis, K., Ryder, U. & Lamond, A. I. The conserved amino-terminal domain of hSRP1 alpha is essential for nuclear protein import. *EMBO J.* **15**, 1818–1825 (1996).
10. Conti, E., Uy, M., Leighton, L., Blobel, G. & Kuriyan, J. Crystallographic analysis of the recognition of a nuclear localization signal by the nuclear import factor karyopherin alpha. *Cell* **94**, 193–204 (1998).
11. Kobe, B., Center, R. J., Kemp, B. E. & Pombourios, P. Crystal structure of human T cell leukemia virus type 1 gp21 ectodomain crystallized as a maltose-binding protein chimera reveals structural evolution of retroviral transmembrane proteins. *Proc. Natl. Acad. Sci. USA* **96**, 4319–4324 (1999).
12. Marford, M. et al. Molecular basis for specificity of nuclear import and prediction of nuclear localization. *Biochim. Biophys. Acta* **1813**, 1562–1577 (2011).
13. Chen, M. H. et al. Phospholipid scramblase 1 contains a nonclassical nuclear localization signal with unique binding site in importin alpha. *J. Biol. Chem.* **280**, 10599–10606 (2005).
14. Takeda, A. A., de Barros, A. C., Chang, C. W., Kobe, B. & Fontes, M. R. Structural basis of importin-alpha-mediated nuclear transport for Ku70 and Ku80. *J. Mol. Biol.* **412**, 226–234 (2011).
15. Chang, C. W., Counago, R. M., Williams, S. J., Boden, M. & Kobe, B. Distinctive conformation of minor site-specific nuclear localization signals bound to importin-alpha. *Traffic* **14**, 1144–1154 (2013).

16. Giesecke, A. & Stewart, M. Novel binding of the mitotic regulator TPX2 (target protein for Xenopus kinesin-like protein 2) to importin- α . *J. Biol. Chem.* **285**, 17628–17635 (2010).
17. Kosugi, S. et al. Six classes of nuclear localization signals specific to different binding grooves of importin α . *J. Biol. Chem.* **284**, 478–485 (2009).
18. Nardozzi, J. D., Lott, K. & Cingolani, G. Phosphorylation meets nuclear import: a review. *Cell Commun. Signal.* **8**, 32 (2010).
19. Fagerlund, R., Kinnunen, L., Kohler, M., Julkunen, I. & Melen, K. NF- κ B is transported into the nucleus by importin α 3 and importin α 4. *J. Biol. Chem.* **280**, 15942–15951 (2005).
20. Fagerlund, R., Melen, K., Cao, X. & Julkunen, I. NF- κ B p52, RelB and c-Rel are transported into the nucleus via a subset of importin α molecules. *Cell Signal.* **20**, 1442–1451 (2008).
21. Sankhala, R. S. et al. Three-dimensional context rather than NLS amino acid sequence determines importin α subtype specificity for RCC1. *Nat. Commun.* **8**, 979 (2017).
22. Ao, Z. et al. Importin α 3 interacts with HIV-1 integrase and contributes to HIV-1 nuclear import and replication. *J. Virol.* **84**, 8650–8663 (2010).
23. Jayappa, K. D., Ao, Z., Yang, M., Wang, J. & Yao, X. Identification of critical motifs within HIV-1 integrase required for importin α 3 interaction and viral cDNA nuclear import. *J. Mol. Biol.* **410**, 847–862 (2011).
24. Smith, K. M. et al. Structural basis for importin α 3 specificity of W proteins in Hendra and Nipah viruses. *Nat. Commun.* **9**, 3703 (2018).
25. Wu, W. et al. Synergy of two low-affinity NLSs determines the high avidity of influenza A virus nucleoprotein NP for human importin α isoforms. *Sci. Rep.* **7**, 11381 (2017).
26. Melen, K. et al. Importin α nuclear localization signal binding sites for STAT1, STAT2, and influenza A virus nucleoprotein. *J. Biol. Chem.* **278**, 28193–28200 (2003).
27. Nardozzi, J., Wenta, N., Yasuhara, N., Vinkemeier, U. & Cingolani, G. Molecular basis for the recognition of phosphorylated STAT1 by importin α 5. *J. Mol. Biol.* **402**, 83–100 (2010).
28. Yasuhara, N. et al. Triggering neural differentiation of ES cells by subtype switching of importin- α . *Nat. Cell Biol.* **9**, 72–79 (2007).
29. Yasuhara, N. et al. Importin α subtypes determine differential transcription factor localization in embryonic stem cells maintenance. *Dev. Cell* **26**, 123–135 (2013).
30. Paciorkowski, A. R. et al. Autosomal recessive mutations in nuclear transport factor KPNA7 are associated with infantile spasms and cerebellar malformation. *Eur. J. Hum. Genet.* **22**, 587–593 (2014).
31. Hayden, M. S. & Ghosh, S. Shared principles in NF- κ B signaling. *Cell* **132**, 344–362 (2008).
32. Oeckinghaus, A. & Ghosh, S. The NF- κ B family of transcription factors and its regulation. *Cold Spring Harb. Perspect. Biol.* **1**, a000034 (2009).
33. Taniguchi, K. & Karin, M. NF- κ B, inflammation, immunity and cancer: coming of age. *Nat. Rev. Immunol.* **18**, 309–324 (2018).
34. Vallabhapurapu, S. & Karin, M. Regulation and function of NF- κ B transcription factors in the immune system. *Annu. Rev. Immunol.* **27**, 693–733 (2009).
35. Sun, S. C. The non-canonical NF- κ B pathway in immunity and inflammation. *Nat. Rev. Immunol.* **17**, 545–558 (2017).
36. Ghosh, G., Wang, V. Y., Huang, D. B. & Fusco, A. NF- κ B regulation: lessons from structures. *Immunol. Rev.* **246**, 36–58 (2012).
37. Chen, F. E., Huang, D. B., Chen, Y. Q. & Ghosh, G. Crystal structure of p50/p65 heterodimer of transcription factor NF- κ B bound to DNA. *Nature* **391**, 410–413 (1998).
38. Huang, D. B., Huxford, T., Chen, Y. Q. & Ghosh, G. The role of DNA in the mechanism of NF κ B dimer formation: crystal structures of the dimerization domains of the p50 and p65 subunits. *Structure* **5**, 1427–1436 (1997).
39. Hart, D. J., Speight, R. E., Sutherland, J. D. & Blackburn, J. M. Analysis of the NF- κ B p50 dimer interface by diversity screening. *J. Mol. Biol.* **310**, 563–575 (2001).
40. Sengchanthalangsy, L. L. et al. Characterization of the dimer interface of transcription factor NF κ B p50 homodimer. *J. Mol. Biol.* **289**, 1029–1040 (1999).
41. Jacobs, M. D. & Harrison, S. C. Structure of an IkappaB α /NF- κ B complex. *Cell* **95**, 749–758 (1998).
42. Huxford, T., Malek, S. & Ghosh, G. Structure and mechanism in NF- κ B/I kappa B signaling. *Cold Spring Harb. Symp. Quant. Biol.* **64**, 533–540 (1999).
43. Rice, N. R., MacKichan, M. L. & Israel, A. The precursor of NF- κ B p50 has I kappa B-like functions. *Cell* **71**, 243–253 (1992).
44. Hoffmann, A., Levchenko, A., Scott, M. L. & Baltimore, D. The IkappaB-NF- κ B signaling module: temporal control and selective gene activation. *Science* **298**, 1241–1245 (2002).
45. Liou, H. C., Nolan, G. P., Ghosh, S., Fujita, T. & Baltimore, D. The NF- κ B p50 precursor, p105, contains an internal I kappa B-like inhibitor that preferentially inhibits p50. *EMBO J.* **11**, 3003–3009 (1992).
46. Zandi, E., Rothwarf, D. M., Delhase, M., Hayakawa, M. & Karin, M. The IkappaB kinase complex (IKK) contains two kinase subunits, IKK α and IKK β , necessary for IkappaB phosphorylation and NF- κ B activation. *Cell* **91**, 243–252 (1997).
47. Coux, O. & Goldberg, A. L. Enzymes catalyzing ubiquitination and proteolytic processing of the p105 precursor of nuclear factor kappaB1. *J. Biol. Chem.* **273**, 8820–8828 (1998).
48. Roff, M. et al. Role of IkappaB α ubiquitination in signal-induced activation of NF κ B in vivo. *J. Biol. Chem.* **271**, 7844–7850 (1996).
49. Henkel, T. et al. Rapid proteolysis of I kappa B- α is necessary for activation of transcription factor NF- κ B. *Nature* **365**, 182–185 (1993).
50. Liang, P. et al. KPNB1, XPO7 and IPO8 mediate the translocation of NF- κ B/p65 into the nucleus. *Traffic* **14**, 1132–1143 (2013).
51. Tao, R. et al. KPNA2 interacts with P65 to modulate catabolic events in osteoarthritis. *Exp. Mol. Pathol.* **99**, 245–252 (2015).
52. Moorthy, A. K. et al. The 20S proteasome processes NF- κ B p105 into p50 in a translation-independent manner. *EMBO J.* **25**, 1945–1956 (2006).
53. Diaz-Garcia, C. et al. Human importin α 3 and its N-terminal truncated form, without the importin- β -binding domain, are oligomeric species with a low conformational stability in solution. *Biochim. Biophys. Acta Gen. Subj.* **1864**, 129609 (2020).
54. Riddick, G. & Macara, I. G. A systems analysis of importin- α - β mediated nuclear protein import. *J. Cell Biol.* **168**, 1027–1038 (2005).
55. Krissinel, E. & Henrick, K. Inference of macromolecular assemblies from crystalline state. *J. Mol. Biol.* **372**, 774–797 (2007).
56. Hayward, S. & Berendsen, H. J. Systematic analysis of domain motions in proteins from conformational change: new results on citrate synthase and T4 lysozyme. *Proteins* **30**, 144–154 (1998).
57. Taylor, D., Cawley, G. & Hayward, S. Quantitative method for the assignment of hinge and shear mechanism in protein domain movements. *Bioinformatics* **30**, 3189–3196 (2014).
58. Jagga, B. et al. Structural basis for nuclear import selectivity of pioneer transcription factor SOX2. *Nat. Commun.* **12**, 28 (2021).
59. Maiti, R., Van Domselaar, G. H., Zhang, H. & Wishart, D. S. SuperPose: a simple server for sophisticated structural superposition. *Nucleic Acids Res.* **32**, W590–W594 (2004).
60. Acerbo, A. S., Cook, M. J. & Gillilan, R. E. Upgrade of MacCHESS facility for X-ray scattering of biological macromolecules in solution. *J. Synchrotron Radiat.* **22**, 180–186 (2015).
61. Zheng, S. Q. et al. MotionCor2: anisotropic correction of beam-induced motion for improved cryo-electron microscopy. *Nat. Methods* **14**, 331–332 (2017).
62. Sankhala, R. S., Lokareddy, R. K. & Cingolani, G. Divergent evolution of nuclear localization signal sequences in herpesvirus terminase subunits. *J. Biol. Chem.* **291**, 11420–11433 (2016).
63. Robbins, J., Dilworth, S. M., Laskey, R. A. & Dingwall, C. Two interdependent basic domains in nucleoplasmic nuclear targeting sequence: identification of a class of bipartite nuclear targeting sequence. *Cell* **64**, 615–623 (1991).
64. Lokareddy, R. K. et al. Distinctive properties of the nuclear localization signals of inner nuclear membrane proteins Heh1 and Heh2. *Structure* **23**, 1305–1316 (2015).
65. Bergqvist, S. et al. Thermodynamics reveal that helix four in the NLS of NF- κ B p65 anchors IkappaB α , forming a very stable complex. *J. Mol. Biol.* **360**, 421–434 (2006).
66. Cervantes, C. F. et al. The RelA nuclear localization signal folds upon binding to IkappaB α . *J. Mol. Biol.* **405**, 754–764 (2011).
67. Latzer, J., Papoian, G. A., Prentiss, M. C., Komives, E. A. & Wolynes, P. G. Induced fit, folding, and recognition of the NF- κ B-nuclear localization signals by IkappaB α and IkappaB β . *J. Mol. Biol.* **367**, 262–274 (2007).
68. Yang, X. D. et al. Negative regulation of NF- κ B action by Set9-mediated lysine methylation of the RelA subunit. *EMBO J.* **28**, 1055–1066 (2009).
69. Huxford, T., Huang, D. B., Malek, S. & Ghosh, G. The crystal structure of the IkappaB α /NF- κ B complex reveals mechanisms of NF- κ B inactivation. *Cell* **95**, 759–770 (1998).
70. Prigent, M., Barlat, I., Langen, H. & Dargemont, C. IkappaB α and IkappaB α /NF- κ B complexes are retained in the cytoplasm through interaction with a novel partner, RasGAP SH3-binding protein 2. *J. Biol. Chem.* **275**, 36441–36449 (2000).
71. Huang, T. T., Kudo, N., Yoshida, M. & Miyamoto, S. A nuclear export signal in the N-terminal regulatory domain of IkappaB α controls cytoplasmic localization of inactive NF- κ B/IkappaB α complexes. *Proc. Natl. Acad. Sci. USA* **97**, 1014–1019 (2000).
72. Johnson, C., Van Antwerp, D. & Hope, T. J. An N-terminal nuclear export signal is required for the nucleocytoplasmic shuttling of IkappaB α . *EMBO J.* **18**, 6682–6693 (1999).
73. Tam, W. F., Lee, L. H., Davis, L. & Sen, R. Cytoplasmic sequestration of rel proteins by IkappaB α requires CRM1-dependent nuclear export. *Mol. Cell. Biol.* **20**, 2269–2284 (2000).

74. Ghosh, S. & Karin, M. Missing pieces in the NF-kappaB puzzle. *Cell* **109**, S81–S96 (2002).
75. Baeuerle, P. A. & Baltimore, D. I kappa B: a specific inhibitor of the NF-kappa B transcription factor. *Science* **242**, 540–546 (1988).
76. Ganchi, P. A., Sun, S. C., Greene, W. C. & Ballard, D. W. A novel NF-kappa B complex containing p65 homodimers: implications for transcriptional control at the level of subunit dimerization. *Mol. Cell. Biol.* **13**, 7826–7835 (1993).
77. Kurland, J. F. et al. NF-kappaB1 (p50) homodimers contribute to transcription of the bcl-2 oncogene. *J. Biol. Chem.* **276**, 45380–45386 (2001).
78. Mizgerd, J. P. et al. Nuclear factor-kappaB p50 limits inflammation and prevents lung injury during *Escherichia coli* pneumonia. *Am. J. Respir. Crit. Care Med.* **168**, 810–817 (2003).
79. Plaksin, D., Baeuerle, P. A. & Eisenbach, L. KBF1 (p50 NF-kappa B homodimer) acts as a repressor of H-2Kb gene expression in metastatic tumor cells. *J. Exp. Med.* **177**, 1651–1662 (1993).
80. Lyman, S. K., Guan, T., Bednenko, J., Wodrich, H. & Gerace, L. Influence of cargo size on Ran and energy requirements for nuclear protein import. *J. Cell Biol.* **159**, 55–67 (2002).
81. Timney, B. L. et al. Simple kinetic relationships and nonspecific competition govern nuclear import rates in vivo. *J. Cell Biol.* **175**, 579–593 (2006).
82. Mitrousis, G., Olia, A. S., Walker-Kopp, N. & Cingolani, G. Molecular basis for the recognition of snurportin 1 by importin beta. *J. Biol. Chem.* **283**, 7877–7884 (2008).
83. McCoy, A. J. Solving structures of protein complexes by molecular replacement with Phaser. *Acta Crystallogr. D Biol. Crystallogr.* **63**, 32–41 (2007).
84. Emsley, P. & Cowtan, K. Coot: model-building tools for molecular graphics. *Acta Crystallogr. D Biol. Crystallogr.* **60**, 2126–2132 (2004).
85. Afonine, P. V. et al. Real-space refinement in PHENIX for cryo-EM and crystallography. *Acta Crystallogr. D Struct. Biol.* **74**, 531–544 (2018).
86. Adams, P. D. et al. PHENIX: building new software for automated crystallographic structure determination. *Acta Crystallogr. D Biol. Crystallogr.* **58**, 1948–1954 (2002).
87. Chen, V. B. et al. MolProbity: all-atom structure validation for macromolecular crystallography. *Acta Crystallogr. D Biol. Crystallogr.* **66**, 12–21 (2010).
88. Hopkins, J. B., Gillilan, R. E. & Skou, S. BioXTAS RAW: improvements to a free open-source program for small-angle X-ray scattering data reduction and analysis. *J. Appl. Crystallogr.* **50**, 1545–1553 (2017).
89. Franke, D. et al. ATSAS 2.8: a comprehensive data analysis suite for small-angle scattering from macromolecular solutions. *J. Appl. Crystallogr.* **50**, 1212–1225 (2017).
90. Svergun, D. I. Determination of the regularization parameter in indirect-transform methods using perceptual criteria. *J. Appl. Crystallogr.* **25**, 495–503 (1992).
91. Grant, T. D. Ab initio electron density determination directly from solution scattering data. *Nat. Methods* **15**, 191–193 (2018).
92. Pettersen, E. F. et al. UCSF Chimera—a visualization system for exploratory research and analysis. *J. Comput. Chem.* **25**, 1605–1612 (2004).
93. Schneidman-Duhovny, D., Hammel, M. & Sali, A. FoXS: a web server for rapid computation and fitting of SAXS profiles. *Nucleic Acids Res.* **38**, W540–W544 (2010).
94. Laskowski, R. A. PDBsum new things. *Nucleic Acids Res.* **37**, D355–D359 (2009).

Acknowledgements

We are thankful to the staff at SSRL beamlines 9-2 and 12-1 and MacCHESS for beamtime at the ID7A1 station and data collection assistance. We also thank Dr. Elizabeth Komives at UCSD for the generous gift of the IκBα expression plasmid. This work was supported by the National Institutes of Health grants R01 GM122844, R35 GM140733, S10 OD017987, and S10 OD023479 to G.C. Research in this publication includes work carried out at the Kimmel Cancer Center X-ray Crystallography and Molecular Interaction Facility at Thomas Jefferson University, which is supported in part by the National Cancer Institute Cancer Center Support Grant P30 CA56036. CHESS is supported by the National Science Foundation grant DMR-1829070, and the MacCHESS resource is supported by the National Institutes of Health grant P30 GM124166-01A1 and NYSTAR.

Author contributions

T.J.F., R.K.L., D.P.Y., R.S.S., and G.C. conceived the project, planned the experiments, and analyzed the data with help from C.O. All SEC–SAXS experiments were performed by R.E.G. who also helped analyzing the data. T.J.F. and G.C. wrote the paper with help from all other authors.

Competing interests

The authors declare no competing interests.

Additional information

Supplementary information The online version contains supplementary material available at <https://doi.org/10.1038/s41467-022-28846-z>.

Correspondence and requests for materials should be addressed to Gino Cingolani.

Peer review information *Nature Communications* thanks Tom Huxford, and the other, anonymous, reviewer(s) for their contribution to the peer review of this work. Peer reviewer reports are available.

Reprints and permission information is available at <http://www.nature.com/reprints>

Publisher's note Springer Nature remains neutral with regard to jurisdictional claims in published maps and institutional affiliations.



Open Access This article is licensed under a Creative Commons Attribution 4.0 International License, which permits use, sharing, adaptation, distribution and reproduction in any medium or format, as long as you give appropriate credit to the original author(s) and the source, provide a link to the Creative Commons license, and indicate if changes were made. The images or other third party material in this article are included in the article's Creative Commons license, unless indicated otherwise in a credit line to the material. If material is not included in the article's Creative Commons license and your intended use is not permitted by statutory regulation or exceeds the permitted use, you will need to obtain permission directly from the copyright holder. To view a copy of this license, visit <http://creativecommons.org/licenses/by/4.0/>.

© The Author(s) 2022